

High Performance Convolution Using Sparsity and Patterns for Inference in Deep Convolutional Neural Networks

Hossam Amer*

Ahmed H. Salamah*

Ahmad Sajedi**

En-hui Yang*

*University of Waterloo

**University of Toronto

{hossam.amer, ahamsalamah, ehyang}@uwaterloo.ca, ahmad.sajedi@mail.utoronto.ca

Abstract

Deploying deep Convolutional Neural Networks (CNNs) is impacted by their memory footprint and speed requirements, which mainly come from convolution. Widely-used convolution algorithms, *im2col* and *MEC*, produce a lowered matrix from an activation map by redundantly storing the map's elements included at horizontal and/or vertical kernel overlappings without considering the sparsity of the map. Using the sparsity of the map, this paper proposes two new convolution algorithms dubbed *Compressed Pattern Overlap (CPO)* and *Compressed Pattern Sets (CPS)* that simultaneously decrease the memory footprint and increase the inference speed while preserving the accuracy. *CPO* recognizes non-zero elements (NZE) at horizontal and vertical overlappings in the activation maps. *CPS* further improves the memory savings of *CPO* by compressing the index positions of neighboring NZEs. In both algorithms, channels/regions of the activation maps with all zeros are skipped. Then, *CPO/CPS* performs convolution via *Sparse Matrix-Vector Multiplication (SpMv)* done on their sparse representations. Experimental results conducted on CPUs show that average per-layer time savings reach up to 63% and *Compression Ratio (CR)* up to 26x with respect to *im2col*. In some layers, our average per layer *CPO/CPS* time savings are better by 28% and *CR* is better by 9.2x than the parallel implementation of *MEC*. For a given CNN's inference, we offline select for each convolution layer the best convolutional algorithm in terms of time between either *CPO* or *CPS* and *im2col*. Our algorithms were selected up to 56% of the non-pointwise convolutional layers. Our offline selections yield CNN inference time savings up to 9% and *CR* up to 10x.

1. Introduction

Deep Convolutional Neural Networks (CNNs) have become the defacto approach for the majority of computer vision tasks. For example, deep CNNs on imageNet classi-

fication dataset have produced an accuracy of 90.2% [34]. Deep CNNs encompass a cascaded and large number of layers that extract features from the input image without any domain knowledge. As the number of these layers continues to grow, CNNs become deeper with increasing memory and computational requirements. These requirements pose certain challenges in deploying deep CNNs in end devices such as mobile phones or IoT devices [15].

Among these many layers are the convolutional layers, which occupy 70-90% of CNN's computational requirements [18]. Currently employed convolution algorithms utilize *General Matrix to Matrix Multiplication (GEMM)* method, where activation maps are transformed into a 2D lowered matrix that is multiplied by a kernel to produce the output feature maps [4, 18, 9].

Lowering-based approaches with *GEMM*, especially *im2col*, are widely-used in current Machine Learning (ML) frameworks due to their efficiency, but they did not fully consider the fact that *Rectifier Linear Unit (ReLU)* is the typical activation function in CNNs [4, 18]. Using *ReLU* leads to sparse activation maps. Experiments carried out on popular CNNs in classification task reveal that 30-50% of convolutional (conv) layers have a density (i.e., portion of *Non-Zero Elements (NZE)*) of activation maps between 0.05 and 0.5 [40, 22]. The lowering-based approaches operate on both zero and NZEs and store them in the lowered matrix, while NZEs are only contributing to the output feature maps. On top of that, both zero elements and NZEs in activation maps included at horizontal and/or vertical kernel overlapping patterns are repetitively stored in the lowered matrix, which create some redundancy. In addition, NZEs in activation maps normally appear near each other, so knowing one *NZE* index and the index pattern of its neighbors can help reconstruct the rest. Moreover, some channels or regions in the activation maps are entirely zero and can be skipped. These insights lead to the question of whether it is possible to utilize activation map's sparsity and patterns to develop fast and memory-efficient algorithms for computing convolution in CNNs.

This paper proposes two convolution algorithms dubbed

Compressed Pattern Overlap (CPO) and Compressed Pattern Sets (CPS) implemented on CPUs that simultaneously decrease the memory footprint and increase the inference speed while preserving the accuracy of deep CNNs. CPO recognizes NZEs at horizontal and vertical overlappings in the activation maps. CPS further improves the memory footprint savings upon CPO by compressing neighboring NZE index positions. Both CPO and CPS also include Skip flags for channels or regions in activation maps that contain no NZEs. After activation map compression, CPO/CPS performs convolution using Sparse Matrix Vector Multiplication (SpMv), where the output resulting from each channel and kernel is performed independently [2].

To apply CPO/CPS to the whole inference process of a given CNN, we observe that the average density at each conv layer is approximately stationary across images. Given a target CNN for inference and a small set of images, we offline select a better convolution method between im2col and our algorithms in terms of time. This results in a hybrid convolution selection method. When applied to the end-to-end inference on the given CNN, the hybrid convolution selection method shows maximum end-to-end inference time savings of 9%, while the average gain in Compression Ratio (CR) across layers go up to 10x. Our contributions are:

- We propose CPO and CPS based on sparsity and patterns of the activation maps with per-layer time savings up to 63%, CR up to 26x with respect to im2col, while maintaining accuracy. (Section 3.1-3.5, 4)
- To the best of our knowledge, this is the first paper that showed both time and space savings obtained from its convolution algorithms in real inference. (Section 2, 4)
- The proposed hybrid convolution selection method provides inference time savings up to 9% and average CR across layers up to 10x. (Section 3.5, 4)

2. Related Work

A wide line of research has been dedicated to compressing and accelerating CNNs by considering sparsity for speed and memory benefits [8, 18, 41, 9, 5, 17, 35, 37, 12, 23]. This line of research can be divided into three main classes. The first class is considering sparsity with focus on dedicated accelerators that use sparsity to overcome its memory challenges [10, 6, 1, 19, 31, 7]. In this paper, we review a subset of papers for the other two classes.

Sparsity of Kernels: Direct sparse convolution in [33, 32] prunes the unnecessary kernel weights in CNNs and stores the non-zero weights in a Compressed Sparse Row (CSR) format in order to perform convolutions while maintaining the accuracy of the CNN classifiers. Furthermore, a three-stage pipeline called deep compression was successfully proposed in [20] where weights are pruned and stored in CSR format, quantized, and then Huffman encoded to reduce the computational requirements of CNNs, but with a

drop of accuracy up to 2.6% in some CNNs. Method in [30] proposed a decomposition of weights where their sparsity is encouraged. Then, convolutions are executed via sparse matrix multiplications during inference time. The papers [3, 16, 29, 27, 28, 21, 25] also focused on kernel sparsity.

Sparsity of Activation Maps: Few papers considered the sparsity of input activation maps although they can play a role in optimizing CNNs due to its relatively larger size than kernel weights. For instance, the approach in [14] successfully induced sparsity to the input maps by retraining using the L1 loss. Then, inputs are quantized, and entropy coded to reduce memory bandwidth. However, the reported speed-up is not in terms of the actual inference time, but rather in terms of the reduction of NZEs in input maps. The method in [11] explored the sparsity of input maps to accelerate inference and was applied to Lidar-based detection or character recognition with reasonable gains. As stated in [11], this method works well in certain tasks or models with a limited and high range of sparsity. Besides, authors in [26] induced $\approx 10\%$ more sparsity on average in CNNs by introducing a threshold-based ReLU activation function and parallelized sparse convolution with noticeable gains in terms of time. However, they did their tests in a sparsity-induced CNN architecture without reporting actual space savings. Furthermore, the method in [36] encoded the input maps via the Coordinate (COO) lists representation and performed convolutions on specific conv layers with density only less than 0.1 without retraining and drop in accuracy. In [13], speed and memory gains over a set of layers were achieved via a CSR-based convolution without considering the horizontal kernel overlapping patterns.

This paper differs from the aforementioned work in three distinct ways: (1) our work considers the sparsity of activation maps rather than kernels. (2) CPO/CPS considers sparsity and patterns such as avoiding repetitive storage of NZEs at horizontal and vertical overlappings, reducing the storage of NZE indices, and skipping all-zero channels or regions. (3) CPO/CPS does not require altering CNNs, do not cause any drops in classification accuracy, deployable in ML frameworks, and provide per-layer CR gains up to 26x and end-to-end inference time savings up to 9%.

3. High Performance Convolution Algorithms

3.1. Sparsity and Patterns Motivation

As defined in Table 1, consider n activation maps with I_c channels. The resulting output with dimensions $I_n \times O_h \times O_w \times K$ from the convolution operation with a kernel W is calculated by:

$$O(n, y, x, k) = \sum_{c=0}^{I_c-1} \sum_{h=0}^{K_h-1} \sum_{w=0}^{K_w-1} I(n, c, y+h, x+w)W(h, w, c, k) \quad (1)$$

where the output spatial dimensions are $O_{h,w} = 1 + \frac{I_{h,w} - K_{h,w}}{s_{h,w}}$. Equation 1 shows that the output feature map at each location (y, x) with a fixed set of kernel weights W is induced by a series of partial sums and multiplications between the input, I , and the kernel, W . Normally, the output is computed using matrix multiplications between a lowered matrix of I and W . As I in typical CNNs is an output of ReLU activation function defined as $\max(0, z)$, it is typically sparse. Zeros in activation maps do not contribute to the output feature maps. Thus, we can reduce the redundancy of activation maps and avoid unnecessary zero computations leading to time/memory savings.

Let us assume a 4x4 kernel with strides 1 and one multi-channel 8x8 input activation map. Lowering-based approaches such as [4, 18] and [9] convert the activation map into a 2D lowered matrix to perform fast matrix multiplication with the kernel. For instance, the default convolution algorithm in the majority of ML frameworks utilizes GEMM using im2col, where inputs are first transformed into a lowered matrix with redundancy. Im2col’s lowered matrix is extracted from patches of the kernel size (4x4), where each patch in each channel is inserted in a separate row of the lowered matrix. New patches are created by shifting the kernel to either right or bottom by a stride of 1. Im2col’s lowered matrix will be relatively large because it repetitively stores a fixed input data value at multiple horizontal and vertical kernel overlappings when this value contributes to the different index positions of the output.

MEC divides I into O_w horizontal partitions with the size of $I_h \times K_w$ where each partition is separated by s_w . For example in the Figure 1 we have 5 horizontal partitions A, B, C, D, and E with the size of 8×4 (e.g., Partition A is $I[0 : 7, 0 : 3]$). Each partition is then converted into a row in the lowered matrix. Hence, elements of I included at horizontal kernel overlapping sites are repeatedly stored at multiple rows of the lowered matrix. For example, the first orange column in I is an overlapping region that overlap horizontally between A, B (overlap2 type). The first blue column has a horizontal overlap between A, B, C (overlap3 type), and the first yellow column has a horizontal overlap between A, B, C, D (overlap4 type). Thus, values of the orange, blue, and yellow columns appear 2, 3, and 4 times, respectively, in the lowered matrix with fixed patterns.

From this discussion, we are motivated to perform convolution via other representations that consider sparsity of I and both the horizontal and vertical patterns. Section 3.2 provides an overview on the components used in CPO/CPS.

3.2. Overview of CPO and CPS

CPO and CPS first split I into O_w horizontal partitions separated by s_w . For each cell in the first partition of I , CPO/CPS assigns a row-major index from 0 to $I_h * K_w - 1$. In partition A of figure 1, we assign indices from 0 to

Table 1: Mathematical Notations for Convolution.

Symbol	Notation	Spatial Dimensions
I	Input	$I_n \times I_h \times I_w \times I_c$
O	Output	$I_n \times O_h \times O_w \times K$
W	Kernel	$K_h \times K_w \times I_c \times K$
s_w, s_h	Kernel stride	

3 for the first row, 4 to 7 for the second row, until 28 to 31 for the last row. In the other partitions, we only assign indices to columns which appear in the new horizontal shift of the kernel window. As a result, we only assign indices in column 4 at partition B. At column 4, we assign the index 3 for the cell at row 0, index 7 for the cell at row 1, and finally the index 31 for the cell at row 7. Partitions C to E follow the exact indexing methodology as partition B.

For CPO and CPS convolution, analysis is done on the nature of conv layers in 6 CNNs used in image classification. Results from the experiment show that 58.5% on average of the convolution layers utilize pointwise convolution. On average, 37.3% of the layers has $s_h = s_w = 1$ and no pointwise convolution. We focus CPO/CPS on non-pointwise kernels whose strides are $s_h = s_w = 1$, but we examine the impact of CPO/CPS on real CNN inference.

To eliminate zero multiplications in convolution, CPO/CPS considers NZEs of I , the horizontal and vertical kernel overlappings. Inspired by CSR, CPO/CPS introduces structures to store the NZEs of I : pointer ptr , data DA , and index IN . For each channel, creation of ptr , DA , and IN is done first for the Non-Overlapping (NOP) regions and then overlap2, overlap3, etc., and overlap K_w regions. To perform convolution, CPO/CPS uses the SpMv between their encoding representations and the kernel. In Section 3.3 and 3.4, we provide a detailed explanation for the ptr , DA , and IN creation and their usage to perform convolution. We assume that $I_n = 1, K = 1$, there are several overlap regions in I ; other cases are straightforward extensions and will be provided in the Supplementary Information (SI). Also, space complexity derivations for CPO and CPS can be found in the SI.

3.3. CPO Encoding and Convolution Algorithms

Given I and its corresponding indices and partitions obtained in Section 3.2, we create ptr , DA , and IN for CPO. Depending on the amount of padding (Pad_Left) on the left of I , CPO skips regions with zero density and starts processing from the next region containing NZEs. In Figure 1, no information for NOP is inserted in all structures because the first and last column in I are all zeros.

The first value of ptr indicates the overlapping type (e.g., 2 for overlap2 type) while the second value represents the number of NZEs in the first column of the given overlap type (e.g., the first orange column of partition A for over-

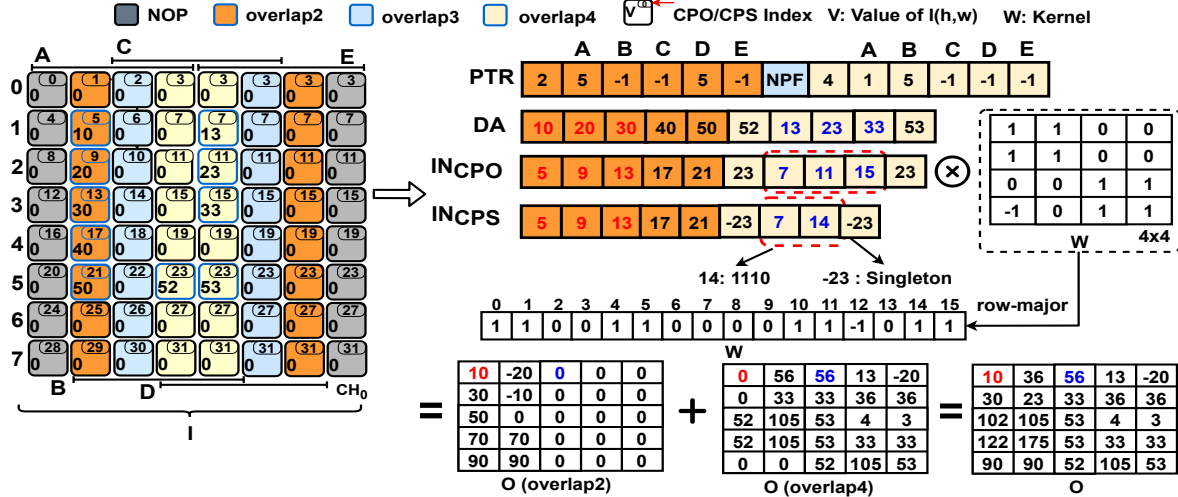


Figure 1: *Left*: Example of input activation map with $I_h = I_w = 8$, $K_h = K_w = 4$, $s_h = s_w = 1$, $I_n = I_c = K = 1$. *Right*: CPO/CPS Encoding and Convolution. Red and blue fonts in IN and DA correspond to their contributions in O .

lap2). Then, we insert the values and indices of NZEs in DA and IN_{cpo} , respectively (e.g., (10, 20, 30, 40, 50) in DA and indices (5, 9, 13, 17, 21) in IN_{cpo}). If the next partitions do not have any new columns in a given overlap type, we insert -1 in ptr and nothing for both DA and IN_{cpo} ; otherwise, we write the cumulative number of NZEs of the given overlap type in ptr and their corresponding NZEs' data values and indices in DA and IN_{cpo} , respectively. In overlap2 for example, the corresponding ptr of partitions B, C, and E are -1. Partition D has 5 in ptr to indicate a new column in overlap2 type, but with no cumulative change in terms of the number of NZEs with respect to partition A. This process repeats for all overlap types which have NZEs (see overlap4 type in Figure 1). For more time/space savings, we insert skip flags in ptr for channels/regions that have only zero elements. No Ptr Flag (NPF) is for overlap regions, and No Ptr Channel (NPC) is for channels.

Algorithm 1 outlines the CPO encoding that consists of three parts. In all three parts, G function inserts the data and corresponding index of NZEs of the given column w in DA and IN vectors, respectively. This function uses nz_ptr to obtain cumulative number of NZEs in the given overlap region. First, lines 11-16 are for NOP, which holds NZEs in activation maps contributing only to the vertical positions of the output (i.e., first and last column in I). Second, lines 17-24 are for overlapping pointers starting from $pType$ until $K_w - 1$ ¹. Third, lines 27-29 are for the overlap K_w region which includes NZEs that contribute K_w times horizontally in the convolution (e.g. yellow columns of overlap4 in Figure 1). In lines 31-37, we determine NPF or NPC flags.

Algorithm 2 performs convolution between the CPO encoding of I and kernel that is done independently for each

channel and kernel. Algorithm 2 decomposes the final output into a summation of partial outputs in each overlap type. We show the partial output from overlap2 ($O(\text{overlap}2)$) and overlap4 ($O(\text{overlap}4)$) in Figure 1, where the final output is the cumulative sum between these partial outputs. The procedure is explained as follows. The kernel is transformed to a row-major vector (see Figure 1). If NOP exists, then we compute the SpMv on the first partition, 0, and the last partition, $O_w - 1$. In Figure 1, NOP does not have NZEs and we skip it (line 15). The rest of the NZEs are processed in the increasing order of the overlap type. In the convSpMv function between lines 1 to 8, each NZE contributes at most $K_h * pType$ to the output, where $pType$ is the overlap type. For example, the first NZE in overlap2 is 10 in DA contributes to four output indices (i.e., $O[0:1][0:1]$). Given the $IN_{CPO}[0]$ corresponding to 10, we compute the two coordinates, y and s , of the output and kernel position (t) based on lines 3 and 4 in Algorithm 2. Except for overlap3 that is skipped by NPF, the rest of the NZEs in overlap2 type follows the steps for 10, and elements in overlap4 follows the process of overlap2, but with $pType=3$. Indexing of ptr , IN , and DA in Algorithm 2 relative to each channel is omitted for simplicity, i.e., line 14 reads the first value of ptr in each channel.

3.4. CPS Encoding and Convolution Algorithms

The goal of CPS is to produce further memory footprint savings over the CPO by exploiting the redundancy of neighbouring NZEs index positions. Over inception and residual CNNs, 81% of the total NZEs appear in the overlap K_w of the activation map that contribute the most to the output feature map. As a result, CPS executes the CPO to obtain ptr and DA . For IN , CPS executes the CPO in all overlap regions except for the overlap K_w region.

To obtain IN_{CPS} from overlap K_w region, CPS groups

¹ $pType = 0$ is for NOP, $pType = 1$ is for overlap2, etc. and $pType = K_w - 1$ is for overlap K_w

Algorithm 1 CPO Encoding Algorithm

```
1: function G( $I, w, Z, ptr, DA, IN, nz\_ptr, ptr\_sh$ )
2: for  $h = 0$  to  $I_h$  do
3:   if  $I(h, w) \neq 0$  then  $DA.insert(I(h, w))$ ,
4:    $IN.insert(Z + (h * K_w))$ ,  $nz\_ptr++$ 
5: procedure CPOENCODE
6: Input:  $I, K_w, Pad\_Left$ 
7: Output:  $ptr, DA, IN$ 
8: Initialize  $ptr\_sh, val\_sh$  to 0
9: for each channel in  $I_c$  do
10:   $nz\_ch, nz\_ptr = 0, pType = Pad\_Left$ 
11:  if  $pType = 0$  then
12:     $nz\_ptr = 0, ptr[ptr\_sh++] = 0, val\_sh = 2$ 
13:    for  $\{w, \hat{w}\}$  in  $\{\{0, 0\}, \{I_w - 1, K_w - 1\}\}$  do
14:       $G(I, w, \hat{w}, ptr, DA, IN, nz\_ptr, ptr\_sh)$ 
15:       $ptr[ptr\_sh++] = nz\_ptr$ 
16:       $nz\_ch += nz\_ptr, pType++$ 
17:       $\tilde{w} = I_w - (pType+1), idx = O_w - pType$ 
18:      for  $w = pType$  to  $K_w - 1$  do
19:         $nz\_ptr = 0, ptr[ptr\_sh++] = pType$ 
20:        for  $\{\bar{w}, \hat{w}\}$  in  $\{\{w, w\}, \{\tilde{w}, \tilde{w} - (idx-1)\}\}$  do
21:           $G(I, \bar{w}, \hat{w}, ptr, DA, IN, nz\_ptr, ptr\_sh)$ 
22:        if  $nz\_ptr > 0$  then
23:           $ptr[ptr\_sh + idx] = nz\_ptr, ptr\_sh += (O_w + 1)$ 
24:        else  $ptr[ptr\_sh - 1] = NPF$   $\triangleright$  If Skip pointer
25:         $nz\_ch += nz\_ptr, pType++, idx++, \tilde{w}--$ 
26:         $idx = 0, ptr[ptr\_sh++] = pType$ 
27:        for  $w = K_w - 1$  to  $I_w - K_w$  do
28:           $G(I, w, w - idx, ptr, DA, IN, nz\_ptr, ptr\_sh)$ 
29:           $ptr[ptr\_sh++] = nz\_ptr, idx++$ 
30:         $nz\_ch += nz\_ptr$ 
31:        if  $nz\_ch=0$  then  $\triangleright$  If Skip Channel
32:           $ptr\_sh -= (K_w-1) + val\_sh - Pad\_Left$ ,
33:           $ptr[ptr\_sh++] = NPC$ ,
34:           $ptr[ptr\_sh : (O_w + val\_sh + 1)] = -1$ 
35:        else if  $nz\_ptr > 0$  then  $ptr\_sh += O_w + 1$ 
36:        else  $ptr[ptr\_sh++] = NPF$ 
37:         $ptr[ptr\_sh : (O_w + val\_sh + 1)] = -1$ 
```

indices obtained in Section 3.2 in a number of sets of size 4, set4. Set4 is a set of 4 indices in the activation map's columns that belongs to overlap K_w region. If I_h is not a multiple of 4, then the last set4 will include the remaining indices and extra zeros to complete the set4. Each set4 can have $2^4 = 16$ index patterns depending on whether the indices inside of the set correspond to zero or non-zero data values. If the number of NZEs in set4 = 4 or 3, we encode the set4 as {first NZE index of the set, pattern}. Here, pattern could be 7 (0111), 11 (1011), 13 (1101), 14 (1110), or 15 (1111). The order of binary representations of each pattern is read from bottom to top in a given column. For

Algorithm 2 CPO Convolution Algorithm

```
1: function CONVSPMV( $K_h, K_w, O_h, pType, x, s, index$ )
2: for  $l = 0$  to  $K_h$  do
3:    $y = (index / K_w) - 1$ 
4:    $t = (index \% K_w + l * K_w)$ 
5:   if  $y \geq 0$  &  $y < O_h$ 
6:      $O[y][s] += DA[x]*W[t]$ 
7:     for  $i = 1$  to  $pType$  do
8:        $O[y][s+i] += DA[x]*W[t-i]$ 
9: procedure CPOALG
10: Input:  $ptr, IN, DA, K_h, K_w, O_h, O_w$ 
11: Output:  $O$ 
12: for each channel in  $I_c$  do
13:   if NPC then Skip channel
14:   Initialize  $ptr\_sh$  to 0
15:    $x = ptr[ptr\_sh]$   $\triangleright$  First value of  $ptr$  in each channel
16:   if  $x = 0$  then
17:     for  $x = ptr[ptr\_sh]$  to  $ptr[ptr\_sh+pType]$  do
18:        $convSpMv(K_h, K_w, O_h, 0, x, 0, IN[x])$ 
19:     for  $x = ptr[ptr\_sh]$  to  $ptr[ptr\_sh+pType]$  do
20:        $convSpMv(K_h, K_w, O_h, 0, x, O_w-1, IN[x])$ 
21:   Skip all pointers with NPF
22:   for  $pType = ptr[ptr\_sh]$  to  $K_w$  do
23:     if NPF then Skip  $ptr$ 
24:      $x = 0$ 
25:     for  $s = 0$  to  $O_w$  do
26:       if  $ptr[ptr\_sh+s+1] < 0$  then
27:          $ptr[ptr\_sh+s+1] = ptr[ptr\_sh+s]$ 
28:         for  $tx = x$  to  $ptr[ptr\_sh+s+1]$  do
29:            $convSpMv(K_h, K_w, O_h, pType, tx, s, IN[tx])$ 
30:          $x = ptr[ptr\_sh+s+1], ptr\_sh++$ 
```

example in Figure 1, the first set4 in the second yellow column is {3, 7, 11, 15} which is encoded to {7, 14}. Here, 14 indicates 3 NZEs out of 4 with order 1110 read from bottom to top. If the number of NZEs in set4 is 2, we insert these two indices in IN_{cps} after multiplying by -1. This multiplication is done to distinguish singletons from the case when set4 has 4 or 3 NZEs. If set4 has one NZE, we encode the singleton after multiplying by -1 (e.g., -23 as a singleton in Figure 1).²

Algorithm 3 executes the all NOP and overlapping types until overlap $K_w - 1$ type as same as Algorithm 1, then CPS encoding executes the overlap K_w region in lines 6-20. We determine the set4's pattern using the pattern variable in Line 10. After recognizing the number of NZEs (nz_col) in the set4, the IN_{CPS} will be encoded either to the first index of the recognized pattern if $nz_col > 2$ as in line 13 or singleton indices will be encoded from auxiliary vector

²Sets of size 4 are chosen to limit the number of pattern possibilities that consequently simplifies index reconstruction.

(Aux) in Lines 15-18.

Algorithm 4 outlines the CPS convolution for overlap K_w region that is done independently for each channel and kernel. In Figure 1, we process overlap4 region, which has 1 NZE in partition A ($ptr[8]$). We read the corresponding index of this NZE i.e., -23. A negative index indicates a singleton that is reconstructed by turning it to positive. As a result, convSpMv is executed for the NZE 52 with index 23. In partition B, we have 4 NZEs ($ptr[9] - ptr[8]$) in DA i.e., 13, 23, 33, and 53. We read the index 7 and pattern 14 from IN_{cps} , so there is 3 NZEs in this pattern. When patterns exist, we reconstruct the original index by adding the starting index with $K_w * nextOffset(pattern, g)$. For pattern 14 or 1110, we process 13 with index 7, 23 with index $7+K_w = 11$, 33 with index $7+K_w*2 = 15$. The last NZE is 53 follows the same practice of the previous singleton (NZE = -23). More details are in Algorithm 4.

Algorithm 3 CPS Encoding Algorithm

```

1: procedure CPSENCODE
2: Input:  $FM, K_w, Pad\_Left$ 
3: Output:  $ptr, DA, IN$ 
4: Initialize Aux[4], nz_col, pattern = 0
5: Insert Lines 10 to 26 From cpoEncode.
6: for  $w = K_w - 1$  to  $I_w - K_w$  do
7:   Reset nz_col, pattern to 0
8:   for  $h = 0$  to  $I_h$  do
9:     if  $I(h, w) \neq 0$  then  $DA.insert(I(h, w))$ ,
10:    pattern +=  $2^{(h\%4)}$ , nz_ptr++
11:    Aux[++nz_col] =  $-1 \times (w - idx + h \times K_w)$ 
12:    if  $nz\_col > 2 \ \& \ (h\%3) = 0$  then
13:       $IN.insert(w - idx + (h - (h\%4)) \times K_w)$ 
14:       $IN.insert(pattern)$ 
15:    else if  $nz\_col = 2 \ \& \ (h\%3) > 1$  then
16:       $IN.insert(Aux[1])$ ,  $IN.insert(Aux[2])$ 
17:    else if  $nz\_col = 1 \ \& \ (h\%3) > 2$  then
18:       $IN.insert(Aux[1])$ 
19:    if  $(h\%3) = 0$  then Reset nz_col, pattern to 0
20:     $ptr[ptr\_sh] = nz\_ptr$ 
21: Insert Lines 29 to 36 From cpoEncode.
```

3.5. Hybrid Inference Over a Target CNN

It is known from the field of linear algebra that the performance of SpMv depends on the input density [32]. The lower the the density, the better SpMv’s performance in time, and vice versa, which makes it challenging to integrate SpMv into all conv layers in real CNN inference. To alleviate this challenge and gain both time and memory savings of CPO/CPS in deep CNN inference, we carried out an experiment where we run 20 images from ImageNet valida-

Algorithm 4 CPS Convolution Algorithm

```

1: procedure CPSALG
2: Input:  $ptr, IN, DA, K_h, K_w, O_h, O_w$ 
3: Output:  $O$ 
4: for each channel in  $I_c$  do
5:   if NPC/NPF then Skip channel/ last ptr
6:    $x = 0$ 
7:   for  $s = 0$  to  $O_w$  do
8:     for  $tx = x$  to  $ptr[ptr\_sh+s+1]$  do.
9:       if  $ptr[ptr\_sh+s+1] < 0$  then
10:         $ptr[ptr\_sh+s+1] = ptr[ptr\_sh+s]$ 
11:        index = tmpIndex =  $IN[tx]$ , pattern = -1
12:        if index < 0 then index =  $IN[tx] = -1 * IN[tx]$ 
13:        else pattern =  $IN[tx+1]$ 
14:        convSpMv( $K_h, K_w, O_h, pType, tx, s, IN[tx]$ )
15:        nnzSet4 = getPatternSize(pattern, tmpIndex)
16:        for  $g = 1$  to  $nnzSet4$  do
17:          index +=  $K_w * nextOffset(pattern, g)$ 
18:          tx = tx + 1
19:          convSpMv( $K_h, K_w, O_h, pType, tx, s, index$ )
20:    $x = ptr[ptr\_sh+s+1], ptr\_sh++$ 
```

tion set through the conv layers of Inception and Residual CNNs. For each conv layer, we record the average density across channels at each image. For ResNet-V2-152, the maximum variance of density over all layers is 0.006, which indicates that the density is approximately stationary from one image to another. This insight is consistent in other CNNs as shown in the SI and intuitive because weights are fixed and should produce stationary characteristics.

Based on this insight, we embedded CPO/CPS into the CNN inference and synergized them using im2col. Suppose that the target CNN used for classification is known. We run our methods along with im2col on the CNN with M images offline. For each layer, we record the total time in convolution of each of three convolution methods over the M ($M=5$) images. For the given CNN, we have two modes of selection: favour time or favour space. Favour time modes selects the convolution method that yields the minimum total time between im2col and CPO, while favour space mode is between im2col and CPS. At inference time, the selected convolution method is used at this conv layer. This selection method results in a hybrid selection of CPO or CPS and im2col over conv layers.

4. Experiments

This section demonstrates the effectiveness of our CPO and CPS written in single threaded C++ in terms of time and memory savings. We report the results relative to im2col used in Caffe framework since im2col is the most popular algorithm [18]. In addition, we wrote the implementation

of CSCC in [13]. Also, same conv layer settings are used to compare CPO/CPS with either COO-based algorithm or MEC implemented in parallel in [36] and [9], respectively. Due to limited resources, 100 randomly sampled images from the ImageNet dataset were used as input stimuli³ [24].

We validate our algorithms on 6 CNNs: IV1, IV3, Inception V4 (IV4), ResNet-V2-50, ResNet-V2-101, and ResNet-V2-152 [39, 40, 38, 22]. From these CNNs, we show two sets of results: 1) per-layer results, 2) end-to-end inference results. For the first set, a sample of 13 conv layers and various characteristics is shown out of 252 conv layers that can be considered by CPO/CPS. We encourage the reader to view the rest of the conv layers results in the SI. To accurately measure the time savings percentage, we calculate the average wall clock time of all algorithms under test after 100 iterations. For the second set, we choose another 5 randomly sampled images for the hybrid convolution selection method. Then, we compute the default total time taken by all types of layers in each CNN under test and compare this time with the total time taken by the selected methods using our proposed hybrid approach. All conv layers not using CPO/CPS are executed using their default implementations. Experiments are carried out on a 16GB memory Quad-Core Intel i7-4790 (3.60 GHz)

CPO/CPS per-layer performance results relative to im2col: Figure 2 shows the performance comparisons in terms of time and memory of CPO and CPS. As shown in this figure, the average CR for CPO and CPS across these layers is 13.3x and 14.7x, respectively. Also, CPO/CPS achieves high per-layer CR savings up to 25.8x. For example, Layer 6 (density of 0.4, 35x35 activation map, and 3x3 kernel) has CR of 23x and 25.8x for CPO/CPS, respectively. For time savings, CPO/CPS may not do well in some layers with high density due to the SpMv memory challenges reported in the literature [39, 32]. For instance, Layer 3 has a density of ≈ 0.6 and our time losses equal to 30% for CPO and 42% for CPS, but our CR gains are 6.9x for CPO and 8.5x for CPS. However, the average time savings of CPO and CPS in these layers is 36% and 27%, respectively. In addition, CPO/CPS achieves on average time savings up to 63.4%. For example, Layer 4 has a density of 0.06 and time savings are 63.4%, 57% for CPO, CPS, respectively. Layer 11 is another example, where the average time saving is 30%, 20% for CPO, CPS, respectively. These savings results are obtained, while preserving the classification accuracy of CNNs under test.

Comparison between CPO/CPS and CSCC: Similar to what’s shown in [13], CSCC’s time saving and CR in layer 4 are better than im2col (35.4% and 13x, respectively). However, supported by Figure 2, CPO/CPS time and memory results in all layers are better than CSCC.

Comparison between CPO/CPS and COO: Inception4e.3 (density=0.1) and Inception5b.3 (density=0.05) in [36] are used to compare our CPO/CPS with COO. In these layers, the average density over 100 images was more than the density reported in [36]. Thus, we choose images in our input stimuli with similar density to [36]. For Inception4e.3 and an image with density 0.16, CPO, CPS, and [36] achieve time savings of 34.3%, 17.5%, 37.1%, respectively, while CR is 16.8x, 17.6x, and 17.2x, respectively. For Inception5b.3 and an image with density 0.05, CPO, CPS, and [36] achieve time savings of 74.5%, 68.6%, 78.89%, respectively, while CR is 31.81x, 32.81x, 27.2x, respectively. For Inception5b.3 and an image with density 0.013, we can achieve time saving of 90.4%, 88.2% and CR of 62.4x, 62.6x for CPO and CPS respectively. From these results, CPO/CPS can outperform the COO in terms of CR with a minor drop in time savings. It is worth noting that we apply our proposed CPO/CPS to real CNN inference and examine CPO/CPS on layers at different densities rather than only at 0.05 and 0.1.

Comparison between CPO/CPS and parallel MEC: Per-layer comparisons are conducted using 4 conv layers already existing in the CNNs under test: cv9, cv10, cv11, cv12 in [9]. MEC performed better in term of time savings in cv9 and cv10, yet CPO/CPS outperformed MEC in terms of CR. We conjecture that these layers do not have enough sparsity degree with respect to their activation map size. For cv11 with density of 0.12, MEC’s time saving is 26.36% and CR is 2.57x, CPO’s time saving is 54.16% and CR is 22.87x, and CPS’s time saving is 44.87% and CR is 23.66x. For cv12 with density of 0.13, MEC’s time saving and CR are 36.97% and 2.16x, respectively. CPO’s time saving for this layer is 37.34%, and CR is 16.16x, while CPS’s time saving is 26.54%, and CR is 16.48x. From these results, CPO/CPS can outperform the parallel MEC’s performance in some layers.

Practical implications of CPO/CPS on CNN Inference: In the first part of Section 4, CPO/CPS improved the performance of im2col in some layers, but with some drops in terms of time savings. Thus, we apply the proposed hybrid convolution selection method in Section 3.5.

Table 2 provides the time savings as well average CR of CPO, CPS, hybrid with CPO and im2col (hybCPO), and hybrid with CPS and im2col (hybCPS). For each CNN, we report time savings in the portion the CPO/CPS is operating (Part) and end-to-end time (E2E) savings. For example, CPO on its own can improve the time of ResNet-V2-101 by 21.4% over the layers CPO is used and by 7.1% in end-to-end. In the same case, the CR is 13.31x/11.9x, respectively. Also, we can observe that there are insignificant time losses in some of the CNNs under test when using only CPO/CPS, but there are CR gains that may be useful for deploying deep CNNs on memory-constrained devices

³During code development, randomized feature maps were generated to verify our results as well.

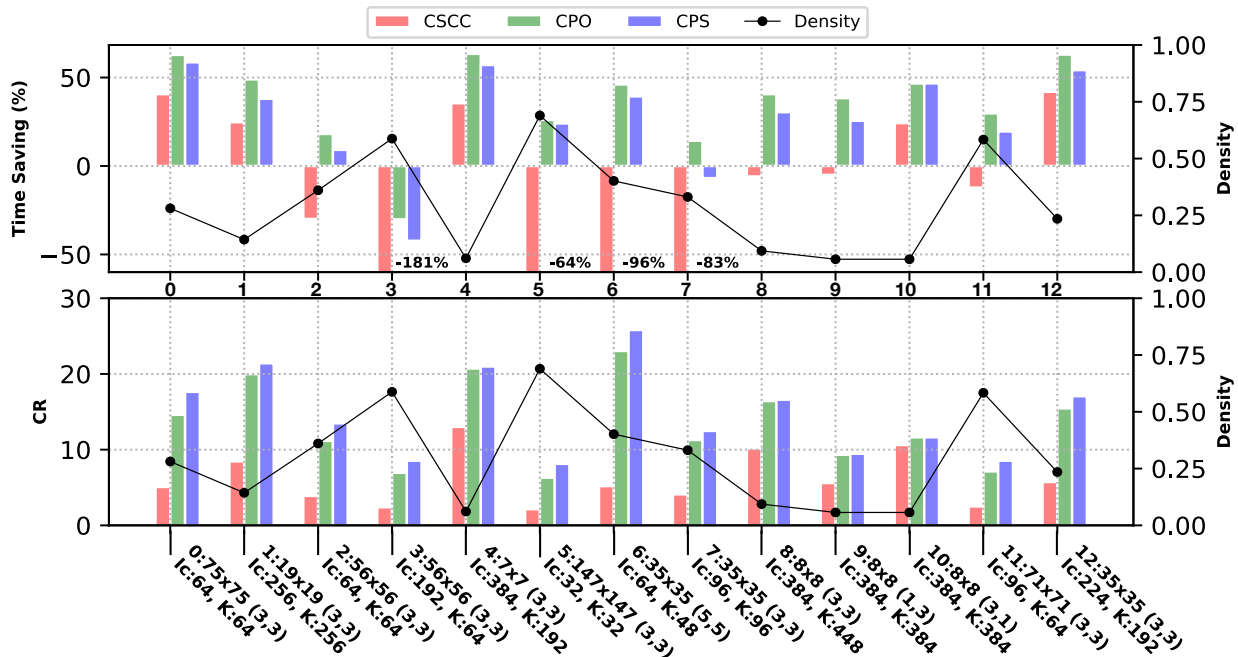


Figure 2: Per-layer Performance Results of CPO, CPS, and CSCC. layers are in this format: layerID: $I_h \times I_w, (K_h \times K_w)$

Table 2: Inference time and memory savings using the proposed hybrid approach based on CPO/CPS. *Part*: Savings in non-pointwise layers with $s_h = s_w = 1$. *E2E*: Overall inference end-to-end savings.

Results \ CNN	Resnet-V2-50		Resnet-V2-101		Resnet-V2-152		IV1		IV3		IV4	
	Part	E2E	Part	E2E	Part	E2E	Part	E2E	Part	E2E	Part	E2E
$T_{cpo}(\%)$	18	6.9	21.4	7.1	12.1	1.8	-15.9	-8	-1	-0.6	-0.5	-0.3
$T_{cps}(\%)$	2.3	1	6.5	2.1	-4.5	-0.7	-35.1	-17.6	-11.8	-7.1	-11.1	-6.1
$T_{hybCPO}(\%)$	20.2	7.8	22.9	7.5	17.9	2.7	9.1	4.6	14.6	8.8	14.7	8
$T_{hybCPS}(\%)$	10.2	4	12.2	4	9.8	1.5	6.6	3.3	9.4	5.7	8.6	4.7
CR_{cpo}	12.2x	9.6x	13.3x	11.9x	13.3x	12.4x	9.4x	9x	9.7x	8.9x	9.7x	9x
CR_{cps}	13.5x	10.5x	14.6x	13x	14.3x	13.2x	10.3x	7.8x	10.3x	9.4x	10.2x	9.47x
CR_{hybCPO}	9.7x	7.7x	11.6x	10.3x	10.3x	9.6x	3.5x	3.4x	6x	5.5x	6.3x	5.9x
CR_{hybCPS}	10.6x	8.4x	9.8x	8.8x	8x	7.4x	2.9x	2.8x	4.8x	4.4x	5.97x	5.6x

with limited bandwidth. Eliminating these losses are done via the hybrid selection approach.

In hybCPO and hybCPS, we calculate the percentage of layers that CPO was selected among the layers that are not pointwise convolution. In hybCPO, CPO was selected with a percentage of 56% on average across CNNs, while CPS was selected with a percentage of 35.5% on average in hybCPS. Hybrid CPO and CPS save inference time with a percentage up to $\approx 9\%$ and up to 6%, respectively, while the average CR across layers of hybCPO and CPS are up to 10.3x and 9x, respectively. CR of hybCPS is less than CPO because it is selected less than CPO, yet hybCPS yields that maximum per-layer CR gains when CPS is selected. These results demonstrate the potential of CPO/CPS in CNN inference.

5. Conclusion and Future Work

This paper proposed CPO and CPS convolution that simultaneously decrease the memory footprint and increase the inference speed while preserving the accuracy. We demonstrated the effectiveness of CPO and CPS with per-layer time savings up to 63% and CR up to 26x with respect to im2col. To the best of our knowledge, this is the first paper that showed both the time and space savings of its algorithms in CNN inference. Using the proposed hybrid convolution selection method, end-to-end inference time savings go up to 9% and CR savings up to 10x. Future extensions could be parallel sparse methods for training/inference on CPUs/GPUs or light-weight CNNs.

References

- [1] Jorge Albericio, Patrick Judd, Tayler Hetherington, Tor Aamodt, Natalie Enright Jerger, and Andreas Moshovos. Cnvlutin: Ineffectual-neuron-free deep neural network computing. *ACM SIGARCH Computer Architecture News*, 44(3):1–13, 2016. [2](#)
- [2] Nathan Bell and Michael Garland. Efficient sparse matrix-vector multiplication on cuda. Technical report, Citeseer, 2008. [2](#)
- [3] Soravit Changpinyo, Mark Sandler, and Andrey Zhmoginov. The power of sparsity in convolutional neural networks. *arXiv preprint arXiv:1702.06257*, 2017. [2](#)
- [4] Kumar Chellapilla, Sidd Puri, and Patrice Simard. High performance convolutional neural networks for document processing. In *Tenth International Workshop on Frontiers in Handwriting Recognition*. Suvisoft, 2006. [1](#), [3](#), [11](#)
- [5] Xuhao Chen. Escoin: Efficient sparse convolutional neural network inference on gpus. *arXiv preprint arXiv:1802.10280*, 2018. [2](#)
- [6] Yu-Hsin Chen, Tushar Krishna, Joel S Emer, and Vivienne Sze. Eyeriss: An energy-efficient reconfigurable accelerator for deep convolutional neural networks. *IEEE journal of solid-state circuits*, 52(1):127–138, 2016. [2](#)
- [7] Yu-Hsin Chen, Tien-Ju Yang, Joel Emer, and Vivienne Sze. Eyeriss v2: A flexible accelerator for emerging deep neural networks on mobile devices. *IEEE Journal on Emerging and Selected Topics in Circuits and Systems*, 9(2):292–308, 2019. [2](#)
- [8] Sharan Chetlur, Cliff Woolley, Philippe Vandermersch, Jonathan Cohen, John Tran, Bryan Catanzaro, and Evan Shelhamer. cudnn: Efficient primitives for deep learning. *arXiv preprint arXiv:1410.0759*, 2014. [2](#)
- [9] Minsik Cho and Daniel Brand. Mec: memory-efficient convolution for deep neural network. In *International Conference on Machine Learning*, pages 815–824. PMLR, 2017. [1](#), [2](#), [3](#), [7](#), [12](#)
- [10] Jason Cong and Bingjun Xiao. Minimizing computation in convolutional neural networks. In *International conference on artificial neural networks*, pages 281–290. Springer, 2014. [2](#)
- [11] Xiao Dong, Lei Liu, Guangli Li, Jiansong Li, Peng Zhao, Xueying Wang, and Xiaobing Feng. Exploiting the input sparsity to accelerate deep neural networks: poster. In *Proceedings of the 24th Symposium on Principles and Practice of Parallel Programming*, pages 401–402, 2019. [2](#)
- [12] R David Evans, Lufei Liu, and Tor M Aamodt. Jpeg-act: accelerating deep learning via transform-based lossy compression. In *2020 ACM/IEEE 47th Annual International Symposium on Computer Architecture (ISCA)*, pages 860–873. IEEE, 2020. [2](#)
- [13] Shengyu Fan, Hui Yu, Dianjie Lu, Shuai Jiao, Weizhi Xu, Fangai Liu, and Zhiyong Liu. Csc: convolution split compression calculation algorithm for deep neural network. *IEEE Access*, 7:71607–71615, 2019. [2](#), [7](#), [12](#), [33](#)
- [14] Georgios Georgiadis. Accelerating convolutional neural networks via activation map compression. In *Proceedings of the IEEE/CVF Conference on Computer Vision and Pattern Recognition*, pages 7085–7095, 2019. [2](#)
- [15] Ian Goodfellow, Yoshua Bengio, and Aaron Courville. *Deep learning*. The MIT Press, 2016. [1](#)
- [16] Yiwen Guo, Anbang Yao, and Yurong Chen. Dynamic network surgery for efficient dnns. *arXiv preprint arXiv:1608.04493*, 2016. [2](#)
- [17] Timo Hackel, Mikhail Usvyatsov, Silvano Galliani, Jan D Wegner, and Konrad Schindler. Inference, learning and attention mechanisms that exploit and preserve sparsity in convolutional networks. *arXiv preprint arXiv:1801.10585*, 2018. [2](#)
- [18] Stefan Hadjis, Firas Abuzaid, Ce Zhang, and Christopher Ré. Caffe con troll: Shallow ideas to speed up deep learning. In *Proceedings of the Fourth Workshop on Data analytics in the Cloud*, pages 1–4, 2015. [1](#), [2](#), [3](#), [6](#)
- [19] Song Han, Xingyu Liu, Huizi Mao, Jing Pu, Ardavan Pedram, Mark A Horowitz, and William J Dally. Eie: Efficient inference engine on compressed deep neural network. *ACM SIGARCH Computer Architecture News*, 44(3):243–254, 2016. [2](#)
- [20] Song Han, Huizi Mao, and William J Dally. Deep compression: Compressing deep neural networks with pruning, trained quantization and Huffman coding. *arXiv preprint arXiv:1510.00149*, 2015. [2](#)
- [21] Babak Hassibi, David G Stork, and Gregory J Wolff. Optimal brain surgeon and general network pruning. In *IEEE international conference on neural networks*, pages 293–299. IEEE, 1993. [2](#)
- [22] Kaiming He, Xiangyu Zhang, Shaoqing Ren, and Jian Sun. Identity mappings in deep residual networks. In *European conference on computer vision*, pages 630–645. Springer, 2016. [1](#), [7](#)
- [23] Torsten Hoefler, Dan Alistarh, Tal Ben-Nun, Nikoli Dryden, and Alexandra Peste. Sparsity in deep learning: Pruning and growth for efficient inference and training in neural networks. *arXiv preprint arXiv:2102.00554*, 2021. [2](#)
- [24] Alex Krizhevsky, Ilya Sutskever, and Geoffrey E Hinton. ImageNet classification with deep convolutional neural networks. In *Advances in neural information processing systems*, pages 1097–1105, 2012. [7](#)
- [25] Souvik Kundu, Mahdi Nazemi, Massoud Pedram, Keith M Chugg, and Peter A Beerel. Pre-defined sparsity for low-complexity convolutional neural networks. *IEEE Transactions on Computers*, 69(7):1045–1058, 2020. [2](#)
- [26] Mark Kurtz, Justin Kopinsky, Rati Gelashvili, Alexander Matveev, John Carr, Michael Goin, William Leiserson, Sage Moore, Nir Shavit, and Dan Alistarh. Inducing and exploiting activation sparsity for fast inference on deep neural networks. In *International Conference on Machine Learning*, pages 5533–5543. PMLR, 2020. [2](#)
- [27] Vadim Lebedev and Victor Lempitsky. Fast convnets using group-wise brain damage. In *Proceedings of the IEEE Conference on Computer Vision and Pattern Recognition*, pages 2554–2564, 2016. [2](#)
- [28] Yann LeCun, John S Denker, Sara A Solla, Richard E Howard, and Lawrence D Jackel. Optimal brain damage. In *NIPs*, volume 2, pages 598–605. Citeseer, 1989. [2](#)

- [29] Hao Li, Asim Kadav, Igor Durdanovic, Hanan Samet, and Hans Peter Graf. Pruning filters for efficient convnets. *arXiv preprint arXiv:1608.08710*, 2016. [2](#)
- [30] Baoyuan Liu, Min Wang, Hassan Foroosh, Marshall Tappen, and Marianna Pinsky. Sparse convolutional neural networks. In *Proceedings of the IEEE conference on computer vision and pattern recognition*, pages 806–814, 2015. [2](#)
- [31] Angshuman Parashar, Minsoo Rhu, Anurag Mukkara, Antonio Puglielli, Rangharajan Venkatesan, Brucek Khailany, Joel Emer, Stephen W Keckler, and William J Dally. Scnn: An accelerator for compressed-sparse convolutional neural networks. *ACM SIGARCH Computer Architecture News*, 45(2):27–40, 2017. [2](#)
- [32] Jongsoo Park, Sheng Li, Wei Wen, Ping Tak Peter Tang, Hai Li, Yiran Chen, and Pradeep Dubey. Faster cnns with direct sparse convolutions and guided pruning. *arXiv preprint arXiv:1608.01409*, 2016. [2](#), [6](#), [7](#)
- [33] Jongsoo Park, Sheng R Li, Wei Wen, Hai Li, Yiran Chen, and Pradeep Dubey. Holistic sparsecnn: Forging the trident of accuracy, speed, and size. *arXiv preprint arXiv:1608.01409*, 1(2), 2016. [2](#)
- [34] Hieu Pham, Qizhe Xie, Zihang Dai, and Quoc V Le. Meta pseudo labels. *arXiv preprint arXiv:2003.10580*, 2020. [1](#)
- [35] Minsoo Rhu, Mike O’Connor, Niladrish Chatterjee, Jeff Pool, Youngeun Kwon, and Stephen W Keckler. Compressing dma engine: Leveraging activation sparsity for training deep neural networks. In *2018 IEEE International Symposium on High Performance Computer Architecture (HPCA)*, pages 78–91. IEEE, 2018. [2](#)
- [36] Shaohuai Shi and Xiaowen Chu. Speeding up convolutional neural networks by exploiting the sparsity of rectifier units. *arXiv preprint arXiv:1704.07724*, 2017. [2](#), [7](#)
- [37] Yuanming Shi, Kai Yang, Tao Jiang, Jun Zhang, and Khaled B Letaief. Communication-efficient edge ai: Algorithms and systems. *IEEE Communications Surveys & Tutorials*, 22(4):2167–2191, 2020. [2](#)
- [38] Christian Szegedy, Sergey Ioffe, Vincent Vanhoucke, and Alexander A Alemi. Inception-v4, inception-resnet and the impact of residual connections on learning. In *Thirty-First AAAI Conference on Artificial Intelligence*, 2017. [7](#)
- [39] Christian Szegedy, Wei Liu, Yangqing Jia, Pierre Sermanet, Scott Reed, Dragomir Anguelov, Dumitru Erhan, Vincent Vanhoucke, and Andrew Rabinovich. Going deeper with convolutions. In *Proceedings of the IEEE conference on computer vision and pattern recognition*, pages 1–9, 2015. [7](#)
- [40] C. Szegedy, V. Vanhoucke, S. Ioffe, J. Shlens, and Z. Wojna. Rethinking the inception architecture for computer vision. In *2016 IEEE Conference on Computer Vision and Pattern Recognition (CVPR)*, pages 2818–2826, June 2016. [1](#), [7](#)
- [41] Wei Wen, Chunpeng Wu, Yandan Wang, Yiran Chen, and Hai Li. Learning structured sparsity in deep neural networks. In *NIPS*, 2016. [2](#)

Supplementary Information

A. Space Complexity Derivations of CPO/CPS

This subsection derives the space complexity of our CPO/CPS encoding representations. Then, we compare CPO/CPS space complexity with im2col, MEC, and CSCC. For each of im2col in subsection 1.1, MEC in subsection 1.2, and CSCC in subsection 1.3, we derive density bounds where the space complexity of our CPO/CPS is better.

The size of Overlapping Pointer (OP) is defined as follows:

$$OP_size = \begin{cases} (1 + O_w) & \text{If } K_w = 1, S_w = 1 \\ (\lceil \frac{K_w}{s_w} \rceil - M)(1 + O_w) & \text{Otherwise} \end{cases} \quad (2)$$

where $M = \max(1, \text{pad_left})$. The size of Non Overlapping Pointer (NOP) is 3 if the padding is VALID. First element indicates NOP type while second and third elements represent the number of NZEs of the first and the last columns, respectively. When the padding is SAME, the size of NOP is zero. The total size of ptr is defined as follows:

$$ptr_size = \sum_{n=1}^{I_n} \sum_{c=1}^{I_c} \max(1, \mathbf{1}_{\rho_{n,c}>0}(NOP_size + OP_size)) - count_{NPF} * (O_w - 1) \quad (3)$$

where $\rho_{n,c}$ is the density of the c th channel of activation map for an image n and $count_{NPF}$ is the total count of NPF skip flags depending on the zero and non-zero elements distribution. The size of DA_{CPO} , DA_{CPS} , and IN_{CPO} are as follows:

$$DA_size_{CPO} = DA_size_{CPS} = IN_size_{CPO} = I_h I_w \sum_{n=1}^{I_n} \sum_{c=1}^{I_c} \rho_{n,c} \quad (4)$$

However the size of the IN_{CPS} is as follows:

$$IN_size_{CPS} = \sum_{n=1}^{I_n} \sum_{c=1}^{I_c} (C'_{1n,c} + 2C'_{2n,c} + 3C'_{3n,c} + 4C'_{4n,c} + C''_{1n,c} + 2C''_{2n,c} + 2C''_{3n,c} + 2C''_{4n,c}) \quad (5)$$

where $C''_{kn,c}$ indicates the number of set4 which has k NZEs inside of the set4 for the c th channel of activation map of an image n in overlap K_w region. $C'_{kn,c}$ represents the number of set4 which has k NZEs inside of the set4 for the c th channel of activation map of an image n in overlap2 type until overlap $(K_w - 1)$ as well as NOP regions.

Finally, the total size of CPO/CPS structure is the summation of their corresponding ptr , DA , and IN sizes.

A.1. Space Complexity Difference between CPO and im2col:

We can define the space complexity of im2col [4], S_{im2col} as follows:

$$S_{im2col} = I_n O_w O_h I_c K_w K_h = I_n (\lceil \frac{I_w - K_w}{s_w} \rceil + 1) (\lceil \frac{I_h - K_h}{s_h} \rceil + 1) I_c K_w K_h. \quad (6)$$

To compute the difference in terms of memory units between im2col, S_{im2col} , and CPO in the worse case, S_{CPO} ($M = 1$, VALID padding, no NPC, no NPF, and $K_w > s_w$), we have:

$$S_{im2col} - S_{CPO} = I_n O_w O_h I_c K_w K_h - I_n I_c \left(3 + (\lceil \frac{K_w}{s_w} \rceil - 1)(1 + O_w) \right) - 2I_h I_w \sum_{n=1}^{I_n} \sum_{c=1}^{I_c} \rho_{n,c} \quad (7)$$

To ensure $S_{im2col} - S_{CPO} \geq 0$, we have to satisfy the following equation:

$$\begin{aligned} 2I_h I_w \sum_{n=1}^{I_n} \sum_{c=1}^{I_c} \rho_{n,c} &\leq I_n O_w O_h I_c K_w K_h + I_n I_c (O_w + 1) - \left(3 + \lceil \frac{K_w}{s_w} \rceil (1 + O_w) \right) I_n I_c \\ \sum_{n=1}^{I_n} \sum_{c=1}^{I_c} \rho_{n,c} &\leq \frac{I_n I_c}{2I_h I_w} \left(O_w (K_w K_h O_h + 1 - \lceil \frac{K_w}{s_w} \rceil) - 2 - \lceil \frac{K_w}{s_w} \rceil \right) \end{aligned} \quad (8)$$

Then, we can deduce the following:

$$\forall_{S_{CPO}, S_{im2col}}(S_{im2col} - S_{CPO}) \geq 0 \Leftrightarrow \exists_{\rho} P(\rho) \quad (9)$$

where $\rho = \sum_{n=1}^{I_n} \sum_{c=1}^{I_c} \rho_{n,c}$ and

$$P(\rho) = \{\rho | 0 \leq \rho \leq \min(1, \max(0, \frac{I_n I_c}{2I_h I_w} \left(O_w(K_w K_h O_h + 1 - \lceil \frac{K_w}{s_w} \rceil) - 2 - \lceil \frac{K_w}{s_w} \rceil \right))\}. \quad (10)$$

A.2. Space Complexity Difference between CPO and MEC:

We can define the space complexity of **Memory Efficient Convolution (MEC)**, S_{MEC} , in [9] as follows:

$$S_{MEC} = I_n O_w K_w I_h I_c = I_n (\lceil \frac{I_w - K_w}{s_w} \rceil + 1) K_w I_h I_c. \quad (11)$$

Now, we compute the difference in terms of memory units between MEC, S_{MEC} , and CPO in the worse case, S_{CPO} ($M = 1$, VALID padding, no NPC, no NPF, and $K_w > s_w$):

$$S_{MEC} - S_{CPO} = I_n I_c O_w K_w I_h - I_n I_c \left(3 + (\lceil \frac{K_w}{s_w} \rceil - 1)(1 + O_w) \right) - 2I_h I_w \sum_{n=1}^{I_n} \sum_{c=1}^{I_c} \rho_{n,c} \quad (12)$$

To ensure $S_{MEC} - S_{CPO} \geq 0$, we have to satisfy the following equation:

$$\begin{aligned} 2I_h I_w \sum_{n=1}^{I_n} \sum_{c=1}^{I_c} \rho_{n,c} &\leq I_n I_c O_w K_w I_h + I_n I_c (O_w + 1) - \left(3 + \lceil \frac{K_w}{s_w} \rceil (1 + O_w) \right) I_n I_c \\ \sum_{n=1}^{I_n} \sum_{c=1}^{I_c} \rho_{n,c} &\leq \frac{I_n I_c}{2I_h I_w} \left(O_w(K_w I_h + 1 - \lceil \frac{K_w}{s_w} \rceil) - 2 - \lceil \frac{K_w}{s_w} \rceil \right) \end{aligned} \quad (13)$$

Then, we can deduce the following:

$$\forall_{S_{CPO}, S_{MEC}}(S_{MEC} - S_{CPO}) \geq 0 \Leftrightarrow \exists_{\rho} P(\rho) \quad (14)$$

where $\rho = \sum_{n=1}^{I_n} \sum_{c=1}^{I_c} \rho_{n,c}$ and

$$P(\rho) = \{\rho | 0 \leq \rho \leq \min(1, \max(0, \frac{I_n I_c}{2I_h I_w} \left(O_w(K_w I_h + 1 - \lceil \frac{K_w}{s_w} \rceil) - 2 - \lceil \frac{K_w}{s_w} \rceil \right))\}. \quad (15)$$

A.3. Space Complexity Difference between CPO and CSCC:

To define the space complexity of **Convolution Split Compression Calculation (CSCC)**, S_{CSCC} , in [13] let's define $\hat{\rho}_i$:

$$\hat{\rho}_i = \frac{\sum_{i=1}^{K_w I_h I_c} \sum_{j=1}^{O_w} \mathbf{1}_{LM_{i,j} \neq 0}}{O_w K_w I_h I_c} \quad (16)$$

where, $\hat{\rho}_i \in [0, 1]$ is the density of the lowered matrix $(LM)_i$.

Based on $\hat{\rho}_i$, we define the density $\hat{\rho}$ for the batch of the lowered matrices for input feature maps as follows:

$$\hat{\rho} = \sum_{i=1}^{I_n} \hat{\rho}_i \quad (17)$$

$$\begin{aligned} S_{CSCC} &= I_n I_c (O_w + 1) + 2 O_w K_w I_h I_c \hat{\rho} \\ &= I_n I_c (\lceil \frac{I_w - K_w}{s_w} \rceil + 2) + 2 (\lceil \frac{I_w - K_w}{s_w} \rceil + 1) K_w I_h I_c \hat{\rho} \end{aligned} \quad (18)$$

For comparison, let us calculate the difference between CSCC, S_{CSCC} , and CPO, S_{CPO} in the worst case ($M = 1$, VALID padding, no NPC, no NPF, and $K_w > s_w$):

$$S_{CSCC} - S_{CPO} = I_n I_c (O_w + 1) + 2 O_w I_h K_w I_c \hat{\rho} - I_n I_c (3 + (\lceil \frac{K_w}{s_w} \rceil - 1)(1 + O_w)) - 2 I_h I_w \sum_{n=1}^{I_n} \sum_{c=1}^{I_c} \rho_{n,c} \quad (19)$$

This difference will be non-negative if and only if,

$$\begin{aligned} 2 I_h (O_w K_w I_c \hat{\rho} - I_w \sum_{n=1}^{I_n} \sum_{c=1}^{I_c} \rho_{n,c}) &\geq -I_n I_c (O_w + 1) (1 - (\lceil \frac{K_w}{s_w} \rceil - 1)) + 3 I_n I_c \\ O_w K_w I_c \hat{\rho} - I_w \sum_{n=1}^{I_n} \sum_{c=1}^{I_c} \rho_{n,c} &\geq \frac{1}{2 I_h} (-I_n I_c (O_w + 1) (2 - \lceil \frac{K_w}{s_w} \rceil)) + 3 I_n I_c \\ -I_w \sum_{n=1}^{I_n} \sum_{c=1}^{I_c} \rho_{n,c} &\geq -O_w K_w I_c \hat{\rho} - \frac{1}{2 I_h} (I_n I_c (O_w + 1) (2 - \lceil \frac{K_w}{s_w} \rceil) - 3 I_n I_c) \\ \sum_{n=1}^{I_n} \sum_{c=1}^{I_c} \rho_{n,c} &\leq \frac{1}{I_w} (O_w K_w I_c \hat{\rho} + \frac{1}{2 I_h} (I_n I_c (O_w + 1) (2 - \lceil \frac{K_w}{s_w} \rceil) - 3 I_n I_c)) \end{aligned} \quad (20)$$

Then, we can deduce the following:

$$\forall_{S_{CPO}, S_{CSCC}} (S_{CSCC} - S_{CPO}) \geq 0 \Leftrightarrow \exists_{\rho} P(\rho) \wedge \exists_{\hat{\rho}} Q(\hat{\rho}) \quad (21)$$

where $\rho = \sum_{n=1}^{I_n} \sum_{c=1}^{I_c} \rho_{n,c}$,

$$P(\rho) = \{\rho | 0 \leq \rho \leq \min(1, \max(0, \frac{1}{I_w} (O_w K_w I_c \hat{\rho} + \frac{1}{2 I_h} (I_n I_c (O_w + 1) (2 - \lceil \frac{K_w}{s_w} \rceil) - 3 I_n I_c))\} \quad (22)$$

, and

$$Q(\hat{\rho}) = \{\hat{\rho} | \hat{\rho} \geq \frac{-I_n I_c (O_w + 1) (2 - \lceil \frac{K_w}{s_w} \rceil) + 3 I_n I_c}{2 O_w I_c I_h K_w}\} \quad (23)$$

For CPS, note the following:

$$\begin{aligned} I_h I_w \sum_{n=1}^{I_n} \sum_{c=1}^{I_c} \rho_{n,c} &= \sum_{n=1}^{I_n} \sum_{c=1}^{I_c} (C'_{1n,c} + 2C'_{2n,c} + 3C'_{3n,c} + 4C'_{4n,c} + C''_{1n,c} + 2C''_{2n,c} + 3C''_{3n,c} + 4C''_{4n,c}) \\ &\geq \sum_{n=1}^{I_n} \sum_{c=1}^{I_c} (C'_{1n,c} + 2C'_{2n,c} + 3C'_{3n,c} + 4C'_{4n,c} + C''_{1n,c} + 2C''_{2n,c} + 2C''_{3n,c} + 2C''_{4n,c}) \end{aligned} \quad (24)$$

which shows that the space savings of CPS relative to im2col can be greater than or equal to the space savings of CPO relative to im2col.

As seen by Equation 24, the space savings of CPS depend on the distribution of the zero and non-zero elements in the activation map. In the previous subsections, we showed that the space savings of CPO could be greater than that of other methods in the literature depending on the density of the activation map, and other spatial properties of the activation map as well as the kernel. This may show indirectly that the space savings of CPS are also greater than other methods in some convolutional layers depending on their characteristics. This can also be verified by the experimental results presented in the paper.

B. Detailed Analysis of our Experimental Results

In the paper, we have already shown a representative sample of per-layer results as well as overall inference results using CPO/CPS in all CNNs under the test. To achieve transparency, this subsection shows all per-layer results in all CNNs under the test of CPO/CPS. Please note that all these layers were already investigated in the paper via the overall inference results. Results in this subsection are reported with respect to im2col for non-point wise convolution layers with $s_h = s_w = 1$.

Tables 3, 4, 5, 6, 7, and 8 show the characteristics of the already considered non-point wise convolution layers with $s_h = s_w = 1$. A row in each table shows the layer ID, the corresponding activation map height (I_h), the corresponding activation map width (I_w), the corresponding output height (O_h), the corresponding output width (O_w), the corresponding kernel height (K_h), the corresponding kernel width (K_w), the corresponding vertical stride (s_h), the corresponding horizontal stride (s_w), the corresponding number of channels (I_c), and the corresponding number of kernels (K).

In Figures 9, 11, 4, 6, the top of Figures 3, 8, we are using a Boxplot to show the behaviour of density per layer through random 20 images. For each layer, we plot a line that consists of a midpoint, a bold line, and a thin line. At any given layer ID, the midpoint shows the mean of the density, the bold line shows the variance of the density, and the thin line shows the density fluctuation of 20 images. As seen by the figures, the density in the majority of the layers is approximately stationary from one image to another. With this observation, the proposed hybrid selection approach was created to integrate the CPO/CPS into CNN inference.

This document presents two sets of figures for time and memory savings for each of CPO, CPS, and CSCC with respect to im2col: (1) At the middle of Figures 3, 8 and the top of Figures 10, 12, 5, 7, we show the per-layer time savings with respect to im2col of the layers already considered by CPO/CPS in all CNNs under test. (2) At the bottom of Figures 3, 8 and the bottom of Figures 10, 12, 5, 7, we show the compression ratio of the layers already considered by CPO/CPS in all CNNs under test. In each Figure, we plot a black line to show the per-layer density. As seen by these figures, CPO/CPS can achieve high time and memory savings in some layers with respect to im2col as already shown in the paper. In addition, we can observe that CPO/CPS is overall better than CSCC as already shown in the paper.

B.1. ResNet-V2-50

Table 3: ResNet-V2-50 DNN Analysis.

ID	Ih	Iw	Oh	Ow	Kh	Kw	Sh	Sw	Ic	K
0	75	75	75	75	3	3	1	1	64	64
1	75	75	75	75	3	3	1	1	64	64
2	38	38	38	38	3	3	1	1	128	128
3	38	38	38	38	3	3	1	1	128	128
4	38	38	38	38	3	3	1	1	128	128
5	19	19	19	19	3	3	1	1	256	256
6	19	19	19	19	3	3	1	1	256	256
7	19	19	19	19	3	3	1	1	256	256
8	19	19	19	19	3	3	1	1	256	256
9	19	19	19	19	3	3	1	1	256	256
10	10	10	10	10	3	3	1	1	512	512
11	10	10	10	10	3	3	1	1	512	512
12	10	10	10	10	3	3	1	1	512	512

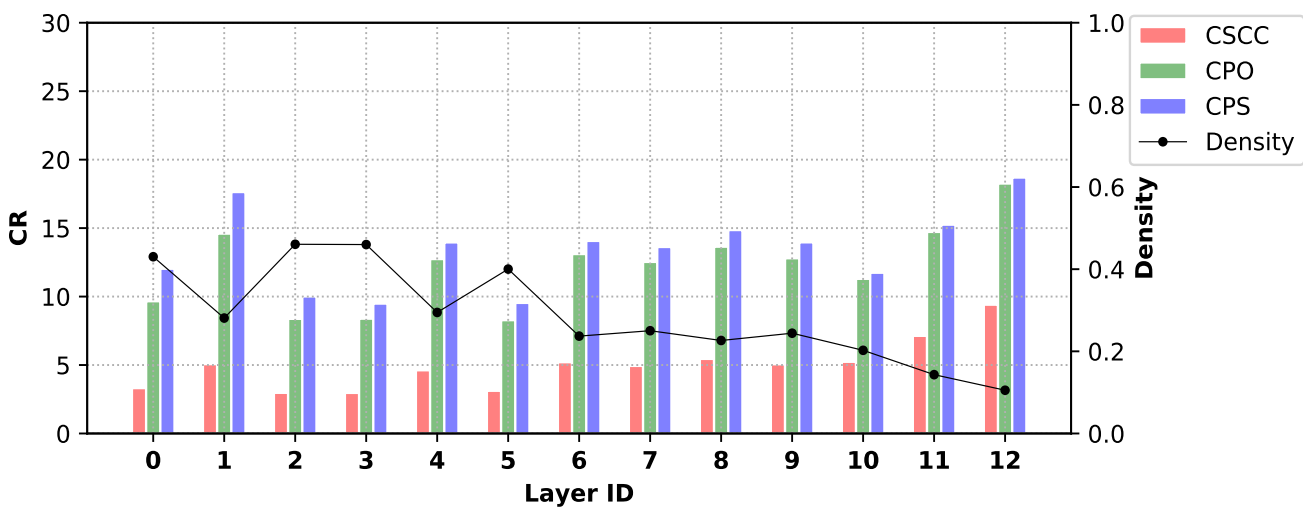
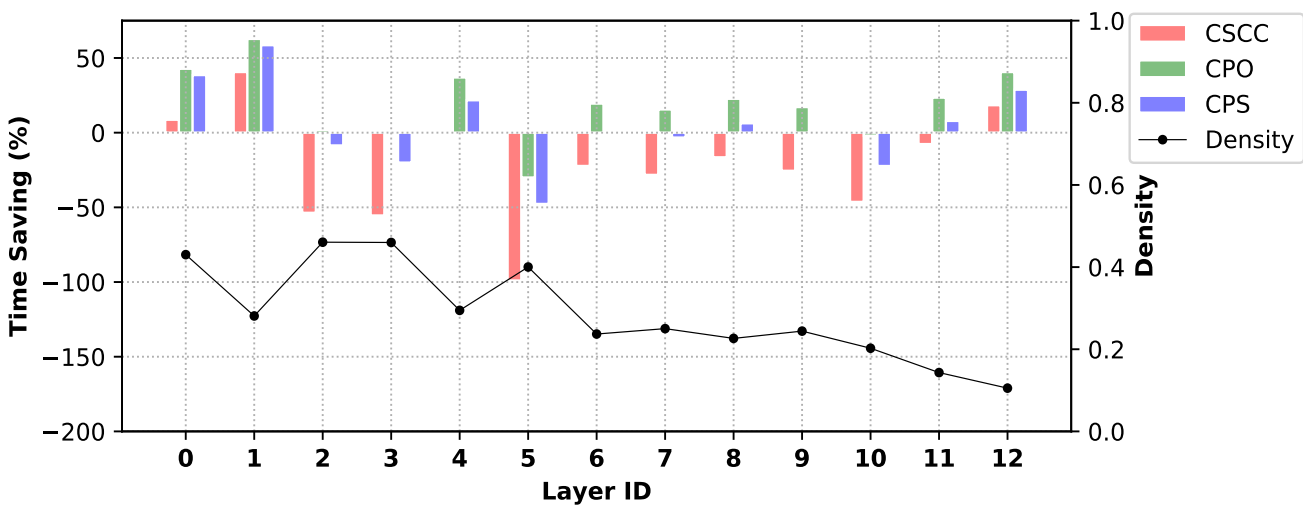
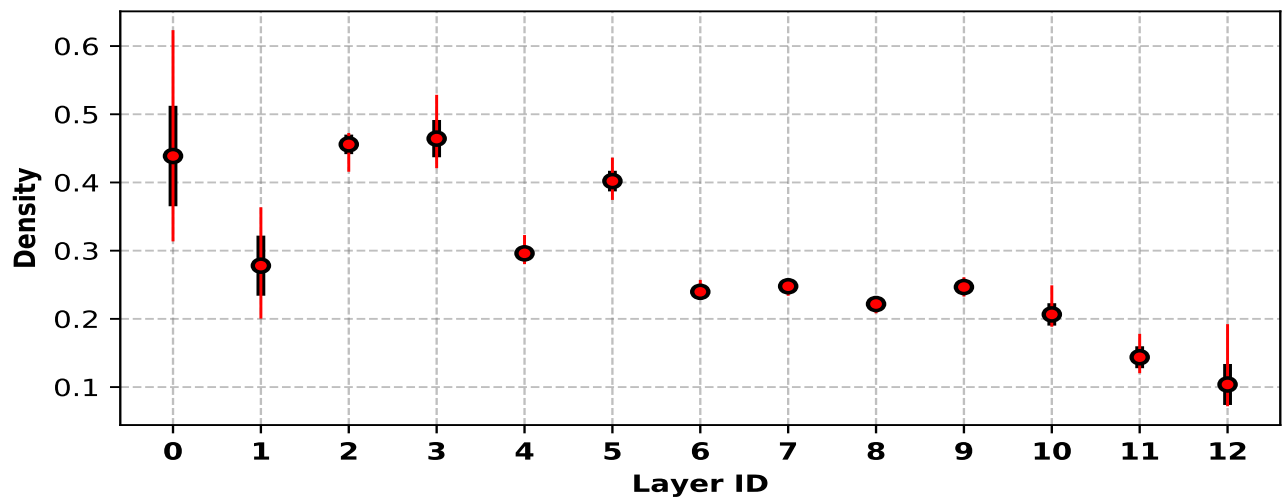


Figure 3: Top to bottom: Per-layer Stationary Density in *ResNet-V2-50* for 20 Images, Per-layer Time Saving Results of CPO, CPS, and CSCC in *ResNet-V2-50* for 100 Images, Per-layer CR Results of CPO, CPS, and CSCC in *ResNet-V2-50* for 100 Images

B.2. ResNet-V2-101

Table 4: ResNet-V2-101 DNN Analysis.

ID	Ih	Iw	Oh	Ow	Kh	Kw	Sh	Sw	Ic	K
0	75	75	75	75	3	3	1	1	64	64
1	75	75	75	75	3	3	1	1	64	64
2	38	38	38	38	3	3	1	1	128	128
3	38	38	38	38	3	3	1	1	128	128
4	38	38	38	38	3	3	1	1	128	128
5	19	19	19	19	3	3	1	1	256	256
6	19	19	19	19	3	3	1	1	256	256
7	19	19	19	19	3	3	1	1	256	256
8	19	19	19	19	3	3	1	1	256	256
9	19	19	19	19	3	3	1	1	256	256
10	19	19	19	19	3	3	1	1	256	256
11	19	19	19	19	3	3	1	1	256	256
12	19	19	19	19	3	3	1	1	256	256
13	19	19	19	19	3	3	1	1	256	256
14	19	19	19	19	3	3	1	1	256	256
15	19	19	19	19	3	3	1	1	256	256
16	19	19	19	19	3	3	1	1	256	256
17	19	19	19	19	3	3	1	1	256	256
18	19	19	19	19	3	3	1	1	256	256
19	19	19	19	19	3	3	1	1	256	256
20	19	19	19	19	3	3	1	1	256	256
21	19	19	19	19	3	3	1	1	256	256
22	19	19	19	19	3	3	1	1	256	256
23	19	19	19	19	3	3	1	1	256	256
24	19	19	19	19	3	3	1	1	256	256
25	19	19	19	19	3	3	1	1	256	256
26	19	19	19	19	3	3	1	1	256	256
27	10	10	10	10	3	3	1	1	512	512
28	10	10	10	10	3	3	1	1	512	512
29	10	10	10	10	3	3	1	1	512	512

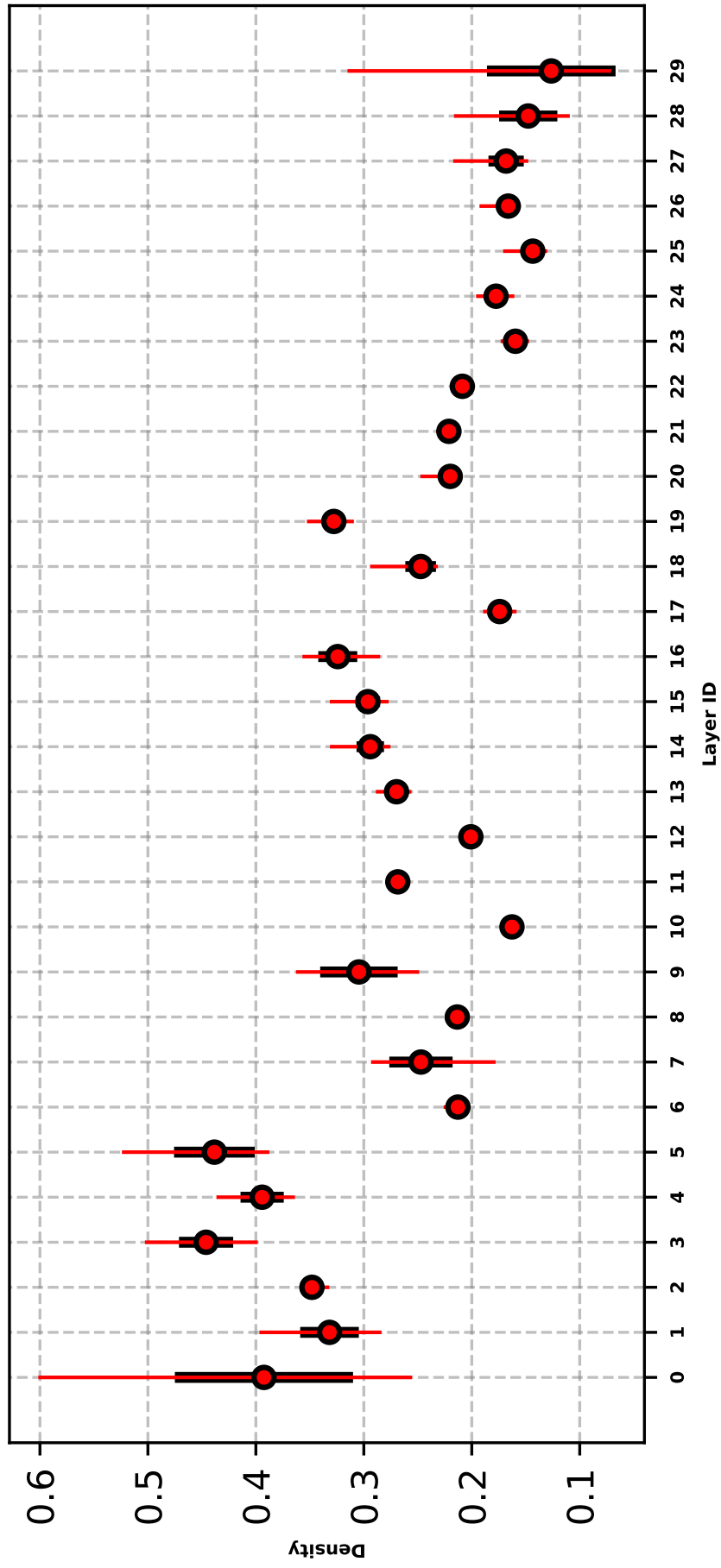


Figure 4: Per-layer Stationary Density in *ResNet-V2-101* for 20 Images

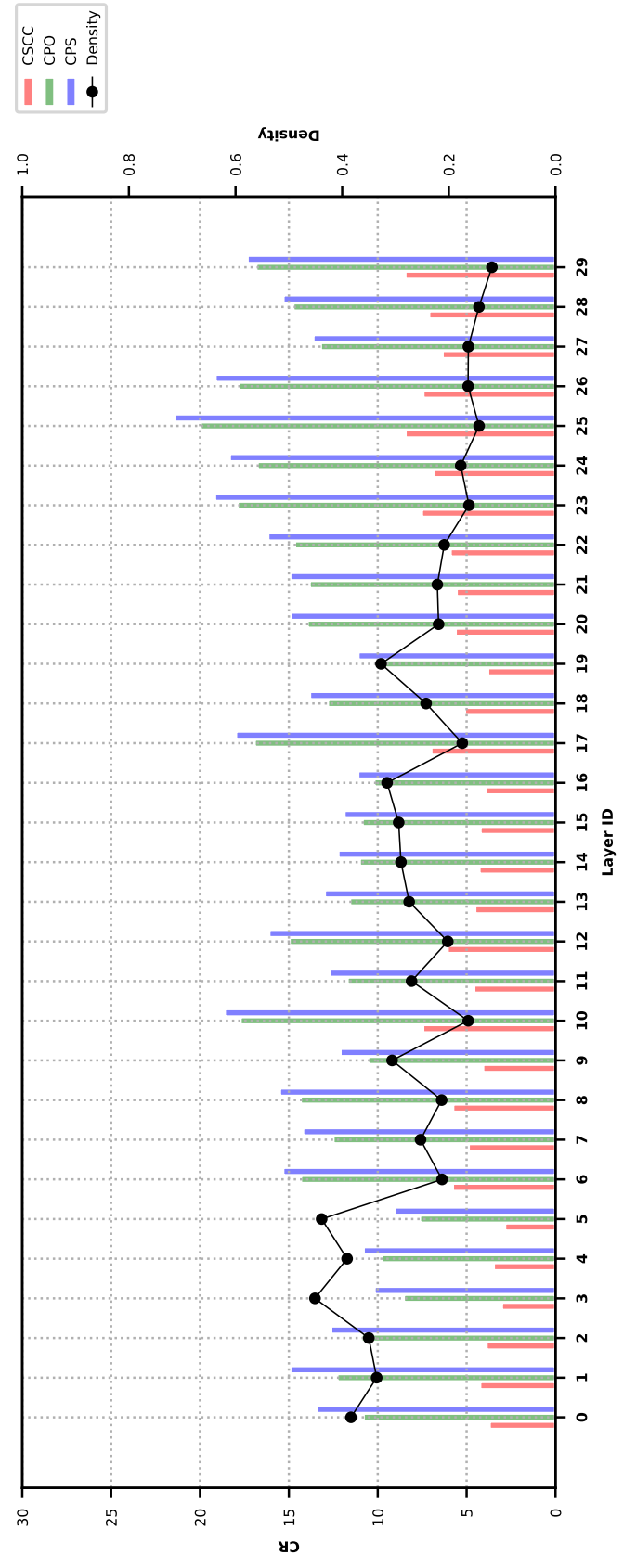
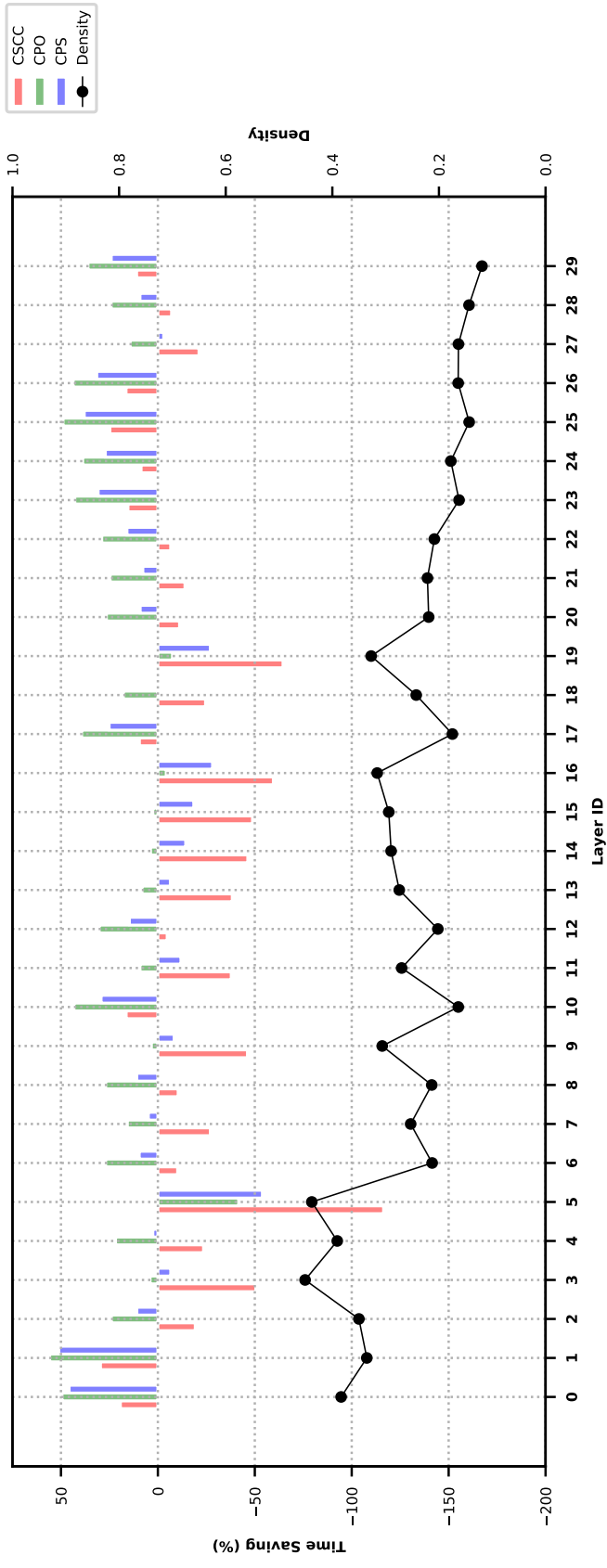


Figure 5: Per-layer Performance Results of CPO, CPS, and CSCC in ResNet-V2-101 for 100 Images

B.3. ResNet-V2-152

Table 5: ResNet-V2-152 DNN Analysis.

ID	Ih	Iw	Oh	Ow	Kh	Kw	Sh	Sw	Ic	K
0	56	56	56	56	3	3	1	1	64	64
1	56	56	56	56	3	3	1	1	64	64
2	28	28	28	28	3	3	1	1	128	128
3	28	28	28	28	3	3	1	1	128	128
4	28	28	28	28	3	3	1	1	128	128
5	28	28	28	28	3	3	1	1	128	128
6	28	28	28	28	3	3	1	1	128	128
7	28	28	28	28	3	3	1	1	128	128
8	28	28	28	28	3	3	1	1	128	128
9	14	14	14	14	3	3	1	1	256	256
10	14	14	14	14	3	3	1	1	256	256
11	14	14	14	14	3	3	1	1	256	256
12	14	14	14	14	3	3	1	1	256	256
13	14	14	14	14	3	3	1	1	256	256
14	14	14	14	14	3	3	1	1	256	256
15	14	14	14	14	3	3	1	1	256	256
16	14	14	14	14	3	3	1	1	256	256
17	14	14	14	14	3	3	1	1	256	256
18	14	14	14	14	3	3	1	1	256	256
19	14	14	14	14	3	3	1	1	256	256
20	14	14	14	14	3	3	1	1	256	256
21	14	14	14	14	3	3	1	1	256	256
22	14	14	14	14	3	3	1	1	256	256
23	14	14	14	14	3	3	1	1	256	256
24	14	14	14	14	3	3	1	1	256	256
25	14	14	14	14	3	3	1	1	256	256
26	14	14	14	14	3	3	1	1	256	256
27	14	14	14	14	3	3	1	1	256	256
28	14	14	14	14	3	3	1	1	256	256
29	14	14	14	14	3	3	1	1	256	256
30	14	14	14	14	3	3	1	1	256	256
31	14	14	14	14	3	3	1	1	256	256
32	14	14	14	14	3	3	1	1	256	256
33	14	14	14	14	3	3	1	1	256	256
34	14	14	14	14	3	3	1	1	256	256
35	14	14	14	14	3	3	1	1	256	256
36	14	14	14	14	3	3	1	1	256	256
37	14	14	14	14	3	3	1	1	256	256
38	14	14	14	14	3	3	1	1	256	256
39	14	14	14	14	3	3	1	1	256	256
40	14	14	14	14	3	3	1	1	256	256
41	14	14	14	14	3	3	1	1	256	256
42	14	14	14	14	3	3	1	1	256	256
43	14	14	14	14	3	3	1	1	256	256
44	7	7	7	7	3	3	1	1	512	512

Continued on next page

Table 5 – continued from previous page

ID	Ih	Iw	Oh	Ow	Kh	Kw	Sh	Sw	Ic	K
45	7	7	7	7	3	3	1	1	512	512
46	7	7	7	7	3	3	1	1	512	512

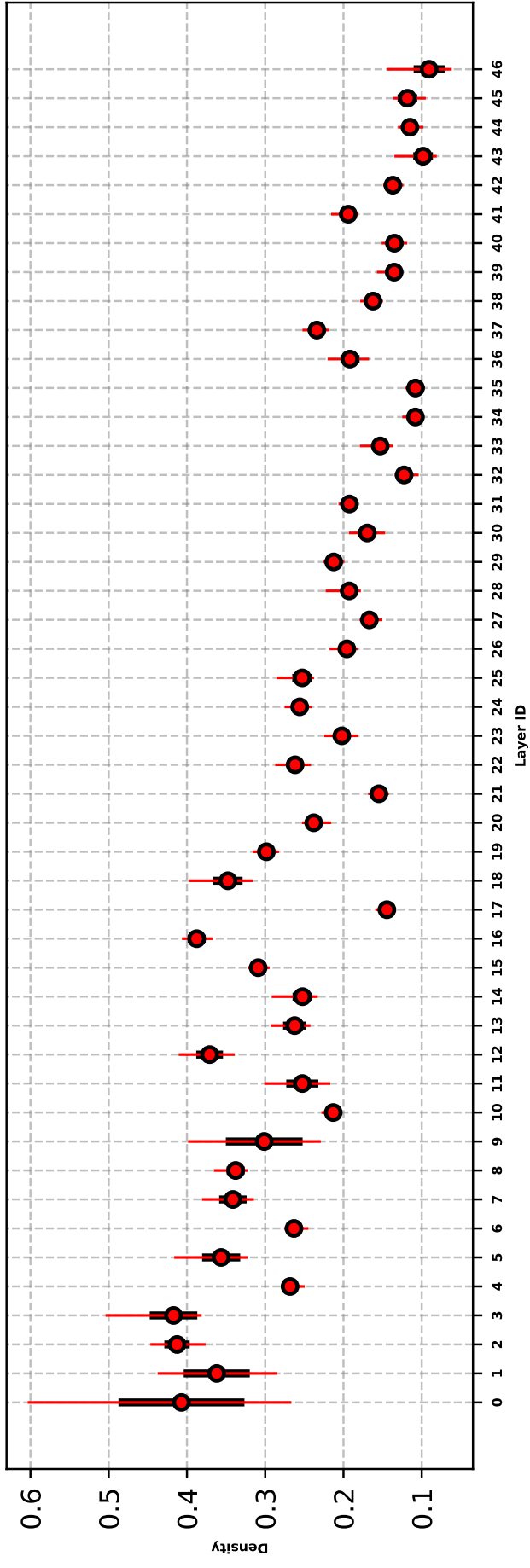


Figure 6: Per-layer Stationary Density in ResNet-V2-152 for 20 images

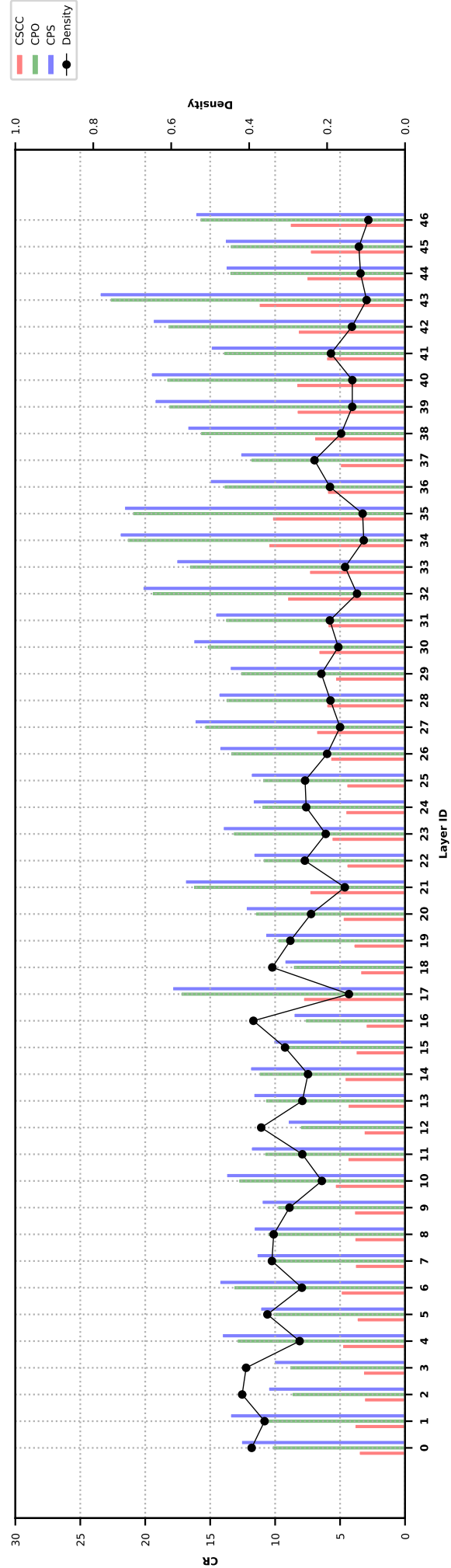
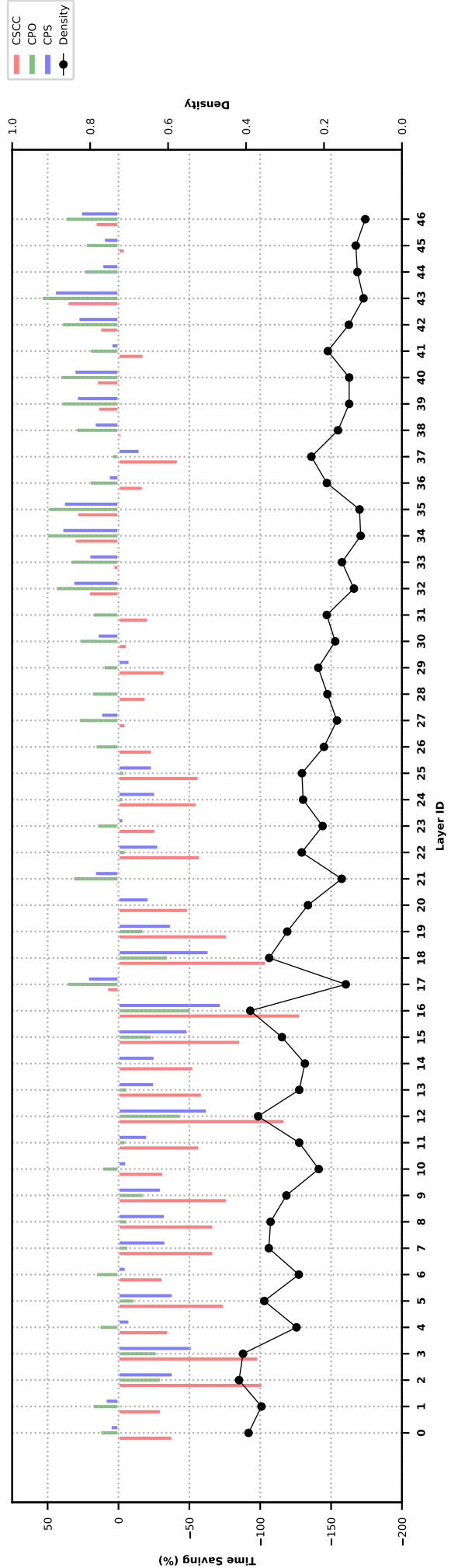


Figure 7: Per-layer Performance Results of CPO, CPS, and CSCC in ResNet-V2-152 for 100 images

B.4. Inception V1 (IV1)

Table 6: IV1 DNN Analysis.

ID	Ih	Iw	Oh	Ow	Kh	Kw	Sh	Sw	Ic	K
0	56	56	56	56	3	3	1	1	64	192
1	28	28	28	28	3	3	1	1	96	128
2	28	28	28	28	3	3	1	1	16	32
3	28	28	28	28	3	3	1	1	128	192
4	28	28	28	28	3	3	1	1	32	96
5	14	14	14	14	3	3	1	1	96	208
6	14	14	14	14	3	3	1	1	16	48
7	14	14	14	14	3	3	1	1	112	224
8	14	14	14	14	3	3	1	1	24	64
9	14	14	14	14	3	3	1	1	128	256
10	14	14	14	14	3	3	1	1	24	64
11	14	14	14	14	3	3	1	1	144	288
12	14	14	14	14	3	3	1	1	32	64
13	14	14	14	14	3	3	1	1	160	320
14	14	14	14	14	3	3	1	1	32	128
15	7	7	7	7	3	3	1	1	160	320
16	7	7	7	7	3	3	1	1	32	128
17	7	7	7	7	3	3	1	1	192	384
18	7	7	7	7	3	3	1	1	48	128

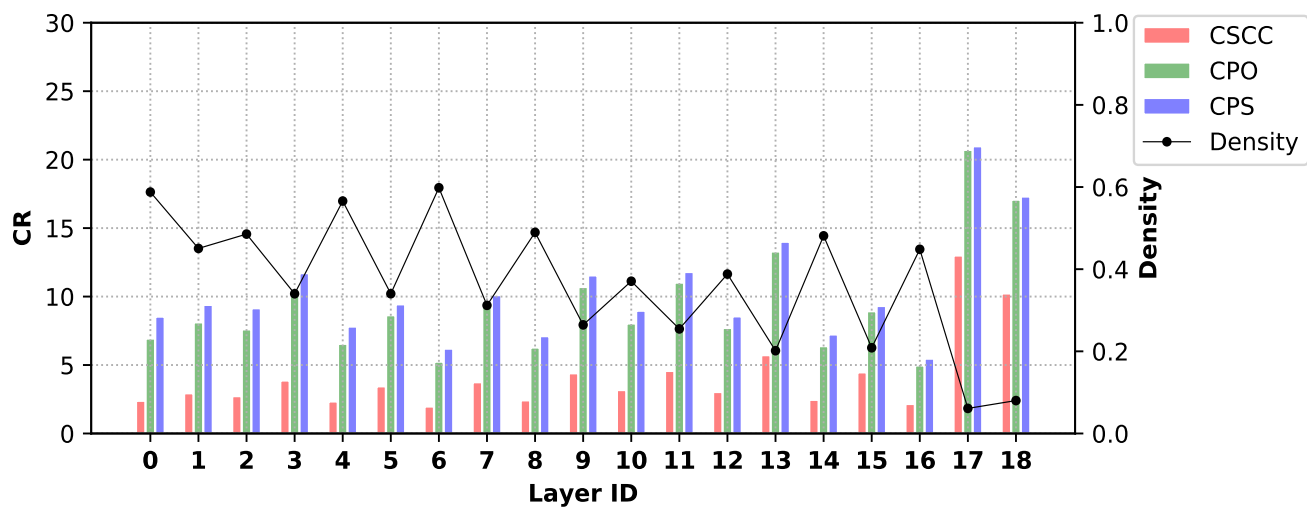
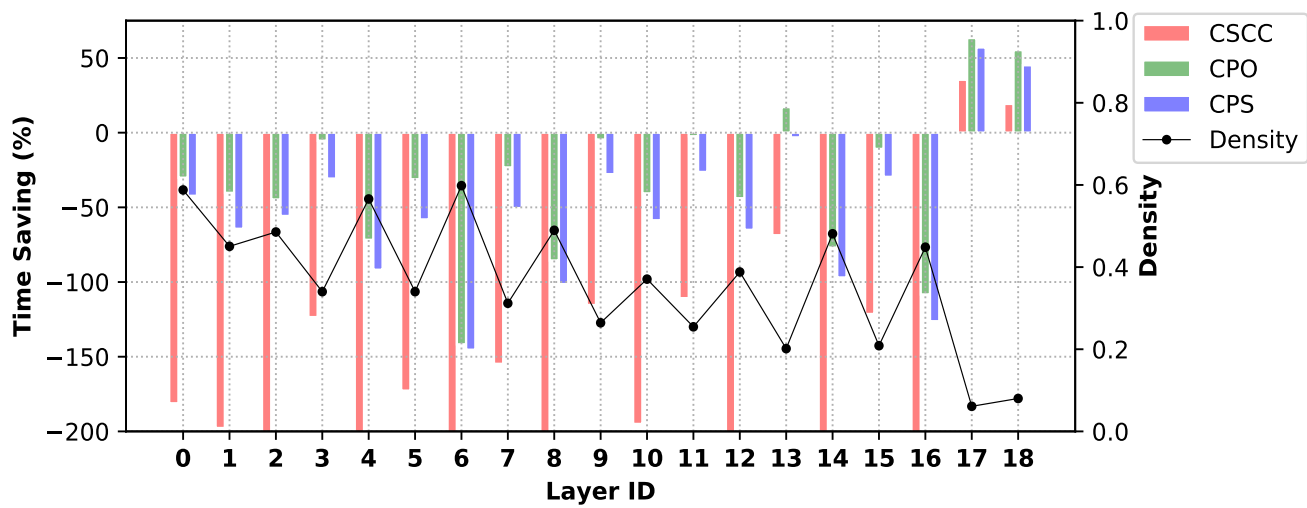
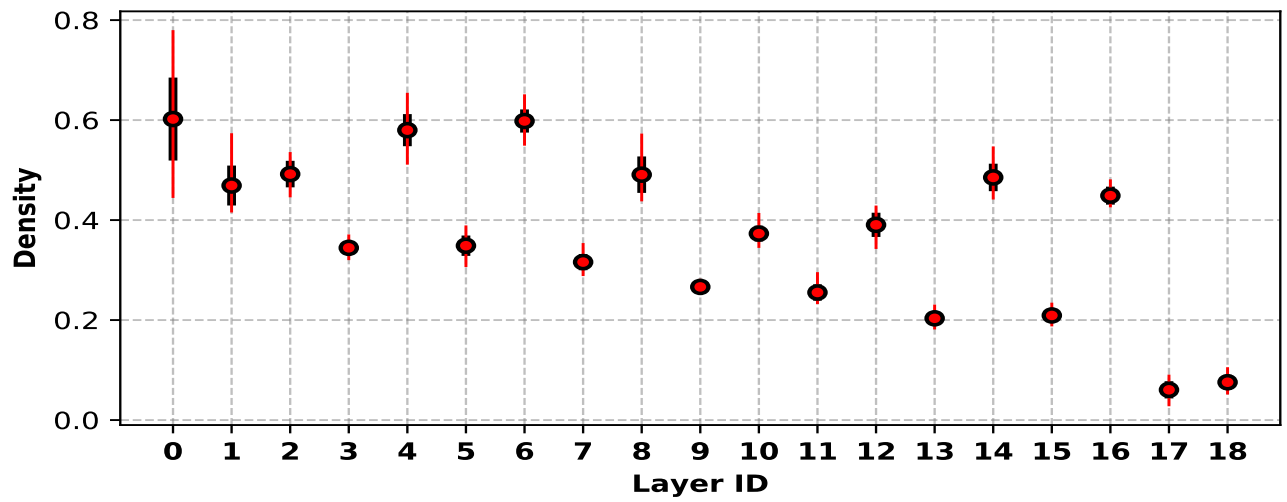


Figure 8: Top to bottom: Per-layer Stationary Density in *IVI* for 20 Images, Per-layer Time Saving Results of CPO, CPS, and CSCC in *IVI* for 100 Images, Per-layer CR Results of CPO, CPS, and CSCC in *IVI* for 100 Images

B.5. Inception V3 (IV3)

Table 7: IV3 DNN Analysis.

ID	Ih	Iw	Oh	Ow	Kh	Kw	Sh	Sw	Ic	K
0	149	149	147	147	3	3	1	1	32	32
1	147	147	147	147	3	3	1	1	32	64
2	73	73	71	71	3	3	1	1	80	192
3	35	35	35	35	5	5	1	1	48	64
4	35	35	35	35	3	3	1	1	64	96
5	35	35	35	35	3	3	1	1	96	96
6	35	35	35	35	5	5	1	1	48	64
7	35	35	35	35	3	3	1	1	64	96
8	35	35	35	35	3	3	1	1	96	96
9	35	35	35	35	5	5	1	1	48	64
10	35	35	35	35	3	3	1	1	64	96
11	35	35	35	35	3	3	1	1	96	96
12	35	35	35	35	3	3	1	1	64	96
13	17	17	17	17	1	7	1	1	128	128
14	17	17	17	17	7	1	1	1	128	192
15	17	17	17	17	7	1	1	1	128	128
16	17	17	17	17	1	7	1	1	128	128
17	17	17	17	17	7	1	1	1	128	128
18	17	17	17	17	1	7	1	1	128	192
19	17	17	17	17	1	7	1	1	160	160
20	17	17	17	17	7	1	1	1	160	192
21	17	17	17	17	7	1	1	1	160	160
22	17	17	17	17	1	7	1	1	160	160
23	17	17	17	17	7	1	1	1	160	160
24	17	17	17	17	1	7	1	1	160	192
25	17	17	17	17	1	7	1	1	160	160
26	17	17	17	17	7	1	1	1	160	192
27	17	17	17	17	7	1	1	1	160	160
28	17	17	17	17	1	7	1	1	160	160
29	17	17	17	17	7	1	1	1	160	160
30	17	17	17	17	1	7	1	1	160	192
31	17	17	17	17	1	7	1	1	192	192
32	17	17	17	17	7	1	1	1	192	192
33	17	17	17	17	7	1	1	1	192	192
34	17	17	17	17	1	7	1	1	192	192
35	17	17	17	17	7	1	1	1	192	192
36	17	17	17	17	1	7	1	1	192	192
37	17	17	17	17	1	7	1	1	192	192
38	17	17	17	17	7	1	1	1	192	192
39	8	8	8	8	1	3	1	1	384	384
40	8	8	8	8	3	1	1	1	384	384
41	8	8	8	8	3	3	1	1	448	384
42	8	8	8	8	1	3	1	1	384	384
43	8	8	8	8	3	1	1	1	384	384
44	8	8	8	8	1	3	1	1	384	384

Continued on next page

Table 7 – continued from previous page

ID	Ih	Iw	Oh	Ow	Kh	Kw	sh	sw	Ic	K
45	8	8	8	8	3	1	1	1	384	384
46	8	8	8	8	3	3	1	1	448	384
47	8	8	8	8	1	3	1	1	384	384
48	8	8	8	8	3	1	1	1	384	384

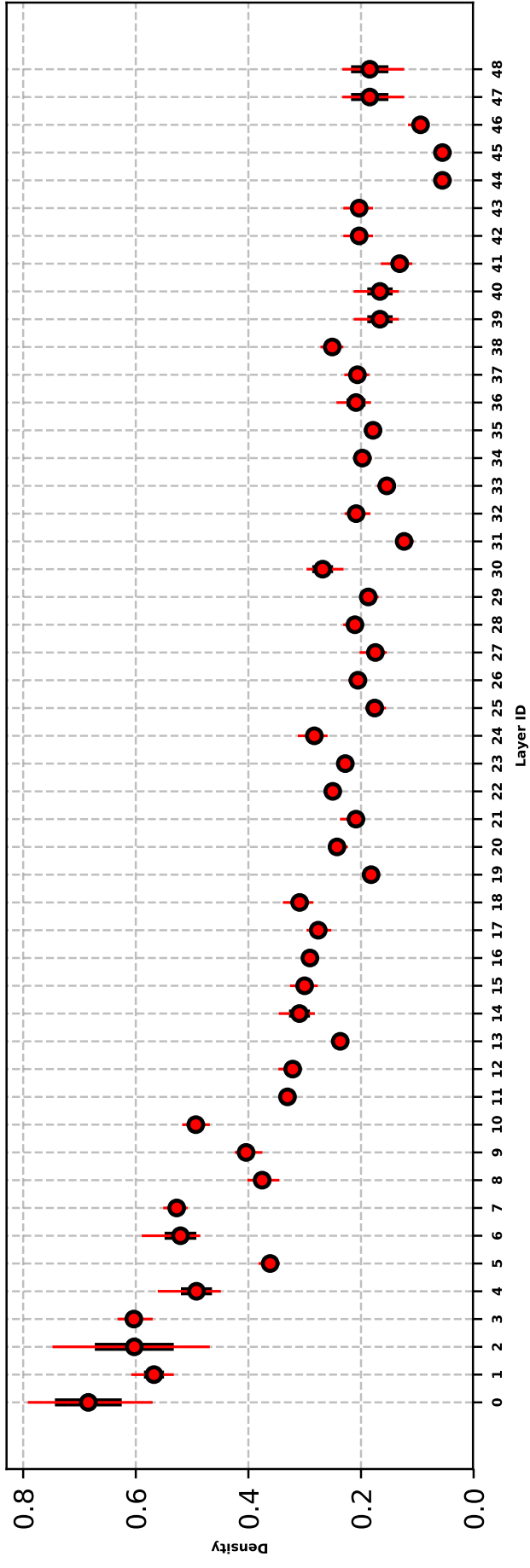


Figure 9: Per-layer Stationary Density in *IV3* for 20 Images

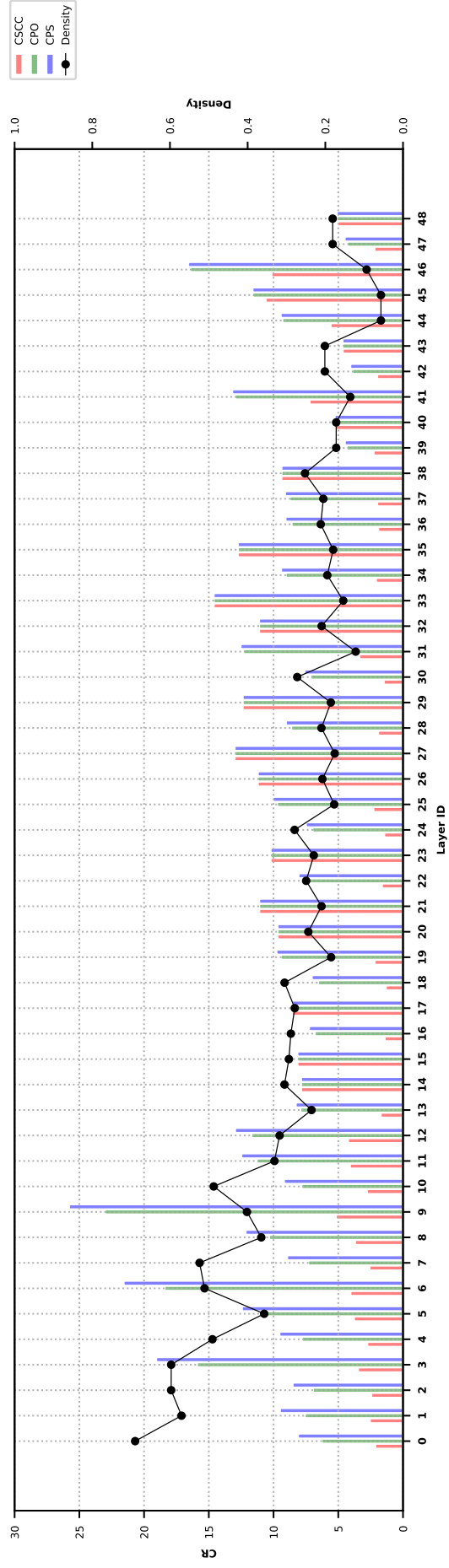
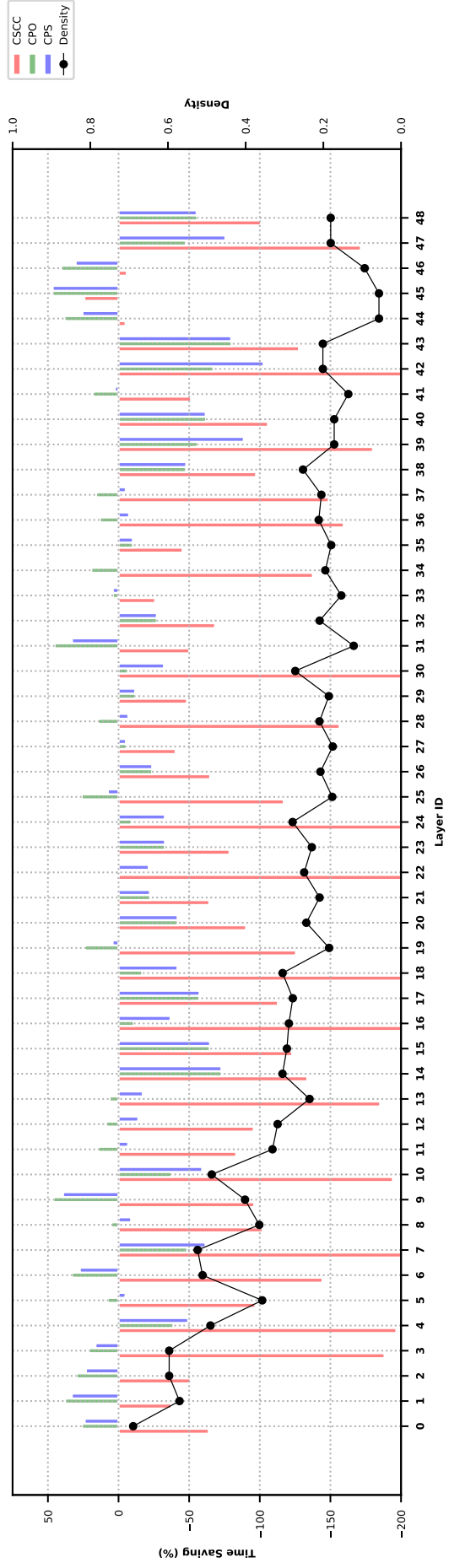


Figure 10: Per-layer Performance Results of CPO, CPS, and CSCC in IV3 for 100 Images

B.6. Inception V4 (IV4)

Table 8: IV4 DNN Analysis.

ID	Ih	Iw	Oh	Ow	Kh	Kw	Sh	Sw	Ic	K
0	149	149	147	147	3	3	1	1	32	32
1	147	147	147	147	3	3	1	1	32	64
2	73	73	71	71	3	3	1	1	64	96
3	73	73	73	73	1	7	1	1	64	64
4	73	73	73	73	7	1	1	1	64	64
5	73	73	71	71	3	3	1	1	64	96
6	35	35	35	35	3	3	1	1	64	96
7	35	35	35	35	3	3	1	1	64	96
8	35	35	35	35	3	3	1	1	96	96
9	35	35	35	35	3	3	1	1	64	96
10	35	35	35	35	3	3	1	1	64	96
11	35	35	35	35	3	3	1	1	96	96
12	35	35	35	35	3	3	1	1	64	96
13	35	35	35	35	3	3	1	1	64	96
14	35	35	35	35	3	3	1	1	96	96
15	35	35	35	35	3	3	1	1	64	96
16	35	35	35	35	3	3	1	1	64	96
17	35	35	35	35	3	3	1	1	96	96
18	35	35	35	35	3	3	1	1	192	224
19	17	17	17	17	1	7	1	1	192	224
20	17	17	17	17	7	1	1	1	224	256
21	17	17	17	17	7	1	1	1	192	192
22	17	17	17	17	1	7	1	1	192	224
23	17	17	17	17	7	1	1	1	224	224
24	17	17	17	17	1	7	1	1	224	256
25	17	17	17	17	1	7	1	1	192	224
26	17	17	17	17	7	1	1	1	224	256
27	17	17	17	17	7	1	1	1	192	192
28	17	17	17	17	1	7	1	1	192	224
29	17	17	17	17	7	1	1	1	224	224
30	17	17	17	17	1	7	1	1	224	256
31	17	17	17	17	1	7	1	1	192	224
32	17	17	17	17	7	1	1	1	224	256
33	17	17	17	17	7	1	1	1	192	192
34	17	17	17	17	1	7	1	1	192	224
35	17	17	17	17	7	1	1	1	224	224
36	17	17	17	17	1	7	1	1	224	256
37	17	17	17	17	1	7	1	1	192	224
38	17	17	17	17	7	1	1	1	224	256
39	17	17	17	17	7	1	1	1	192	192
40	17	17	17	17	1	7	1	1	192	224
41	17	17	17	17	7	1	1	1	224	224
42	17	17	17	17	1	7	1	1	224	256
43	17	17	17	17	1	7	1	1	192	224
44	17	17	17	17	7	1	1	1	224	256

Continued on next page

Table 8 – continued from previous page

ID	Ih	Iw	Oh	Ow	Kh	Kw	Sh	Sw	Ic	K
45	17	17	17	17	7	1	1	1	192	192
46	17	17	17	17	1	7	1	1	192	224
47	17	17	17	17	7	1	1	1	224	224
48	17	17	17	17	1	7	1	1	224	256
49	17	17	17	17	1	7	1	1	192	224
50	17	17	17	17	7	1	1	1	224	256
51	17	17	17	17	7	1	1	1	192	192
52	17	17	17	17	1	7	1	1	192	224
53	17	17	17	17	7	1	1	1	224	224
54	17	17	17	17	1	7	1	1	224	256
55	17	17	17	17	1	7	1	1	192	224
56	17	17	17	17	7	1	1	1	224	256
57	17	17	17	17	7	1	1	1	192	192
58	17	17	17	17	1	7	1	1	192	224
59	17	17	17	17	7	1	1	1	224	224
60	17	17	17	17	1	7	1	1	224	256
61	17	17	17	17	1	7	1	1	256	256
62	17	17	17	17	7	1	1	1	256	320
63	8	8	8	8	1	3	1	1	384	256
64	8	8	8	8	3	1	1	1	384	256
65	8	8	8	8	3	1	1	1	384	448
66	8	8	8	8	1	3	1	1	448	512
67	8	8	8	8	1	3	1	1	512	256
68	8	8	8	8	3	1	1	1	512	256
69	8	8	8	8	1	3	1	1	384	256
70	8	8	8	8	3	1	1	1	384	256
71	8	8	8	8	3	1	1	1	384	448
72	8	8	8	8	1	3	1	1	448	512
73	8	8	8	8	1	3	1	1	512	256
74	8	8	8	8	3	1	1	1	512	256
75	8	8	8	8	1	3	1	1	384	256
76	8	8	8	8	3	1	1	1	384	256
77	8	8	8	8	3	1	1	1	384	448
78	8	8	8	8	1	3	1	1	448	512
79	8	8	8	8	1	3	1	1	512	256
80	8	8	8	8	3	1	1	1	512	256

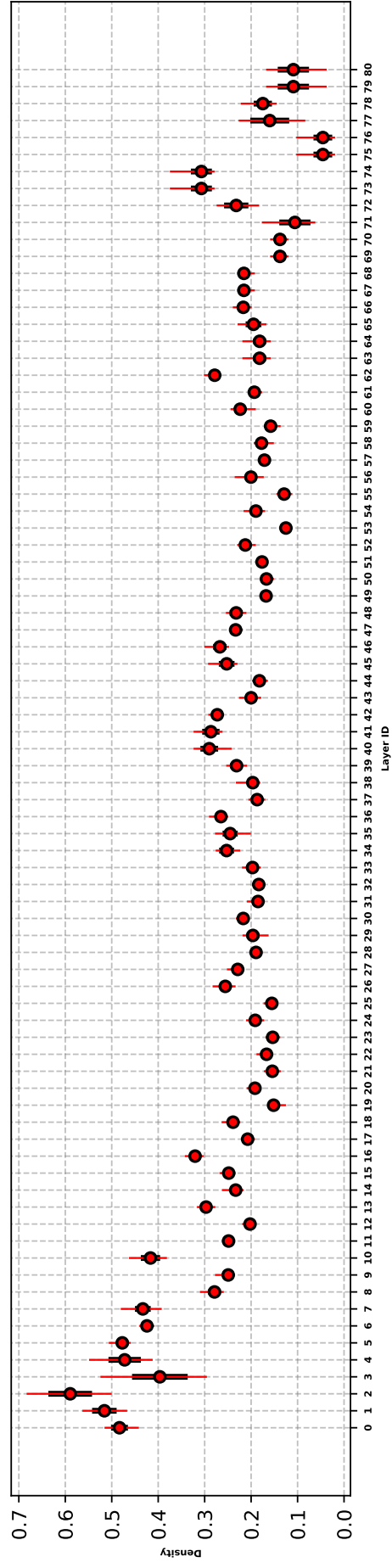


Figure 11: Per-layer Stationary Density in $W4$ for 20 Images

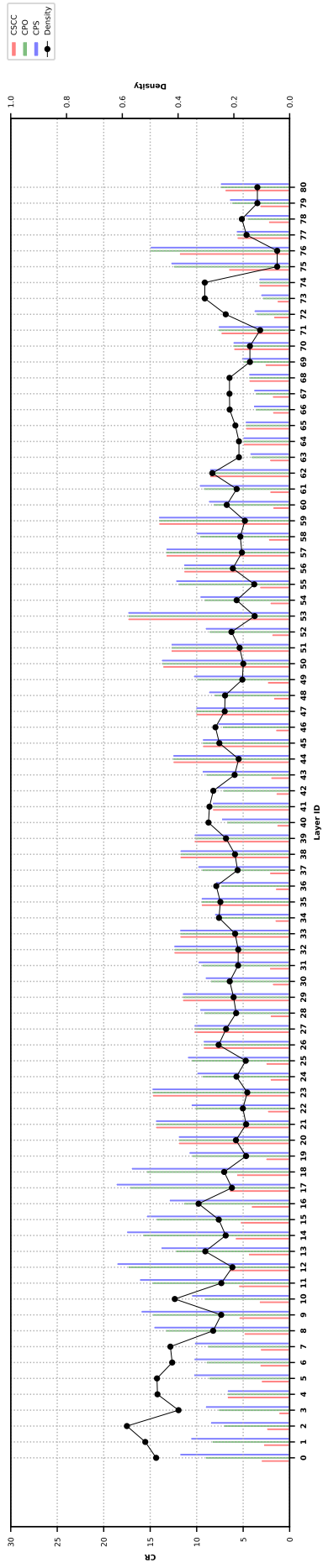
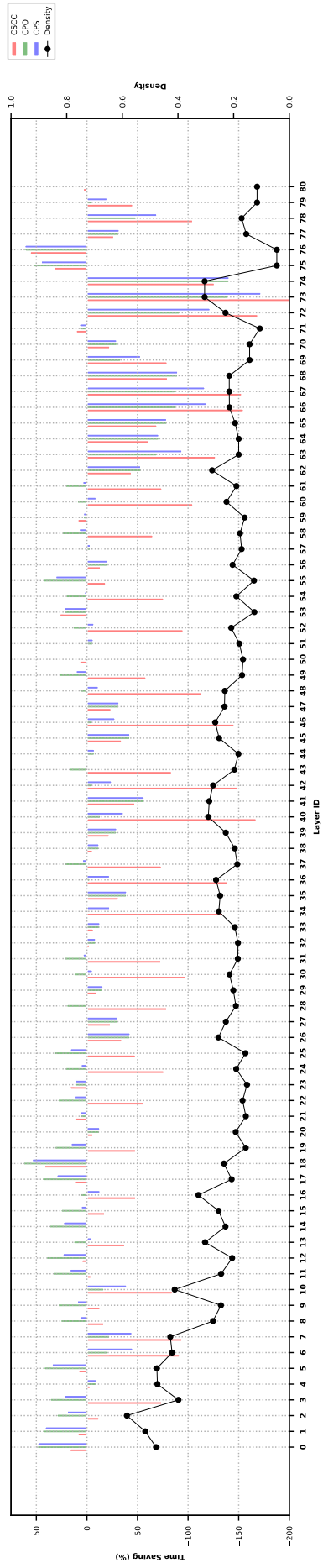


Figure 12: Per-layer Performance Results of CPO, CPS, and CSCC in *IV4* for 100 images

C. CPO/CPS Encoding and Convolution Algorithms for $K_w = 1$

This subsection outlines the encoding and convolution algorithms for the proposed CPO for the special case $K_w = 1$ (i.e., there are no overlap regions). This case is a straightforward extension of the algorithms presented in the paper (e.g., Layer 10 in the paper). Results for this case have already been presented in the paper, but we are providing the algorithms for this special case for clarity reasons. In addition, please note we chose to run CPO when $K_w = 1$ between CPO and CPS because of more overall time saving. In Algorithm 5, we simplify the complexity of the CSCC encoder in [13] in terms of implementation as their algorithm is designed for any value of K_w and s_w . Also, we added NPC in the CPO encoder to skip channels with all zeros. Algorithm 6 is mainly similar to the convolution algorithm presented in [13], but with NPC support to skip the computations and storage of channels with all zeros.

Algorithm 5 CPO/CPS Encoding Algorithm $K_w = 1$

```

1: procedure CPOENCODE
2:   Input:  $I, K_w, O_w$ 
3:   Output:  $ptr, DA, IN$ 
4:   Initialize  $ptr\_sh, val\_sh, s$  to 0
5:   for each channel in  $I_c$  do
6:      $nz\_ch, nz\_ptr, s = 0$ 
7:      $ptr[ptr\_sh++] = 0$ 
8:     for  $w = 0$  to  $I_w$  do
9:       if  $I(h, w) \neq 0$ 
10:         $DA.insert(I(h, w))$ 
11:         $IN.insert(w + (h * K_w) - s)$ 
12:         $nz\_ptr++$ 
13:      if  $w = s + K_w - 1$  ▷ If End Submatrix
14:         $h++$ 
15:         $w = s - 1$ 
16:      if  $h = I_h$ 
17:         $h = 0$ 
18:         $s++$ 
19:         $w = s - 1$ 
20:         $ptr[ptr\_sh++] = nz\_ptr$ 
21:      if  $w = I_w - K_w$ 
22:        Break Loop ▷ End of Channel
23:    if  $nz\_ptr = 0$  ▷ If Skip Channel
24:       $ptr\_sh -= (O_w + 1)$ 
25:       $ptr[ptr\_sh++] = NPC$ 

```

Algorithm 6 CPO/CPS Convolution Algorithm $K_w = 1$

```
1: function CONVSPMV( $K_h, K_w, O_h, x, s, \text{index}$ )
2:   for  $l = 0$  to  $K_h$  do
3:      $y = (\text{index} / K_w) - 1$ 
4:      $t = (\text{index} \% K_w + l * K_w)$ 
5:     if  $y \geq 0$  &  $y < O_h$ 
6:        $O[y][s] += DA[x]*W[t]$ 
7: procedure CPOALG
8:   Input:  $ptr, IN, DA, K_h, K_w, O_h, O_w$ 
9:   Output:  $O$ 
10:  Initialize  $ptr\_sh = 0$ 
11:  for each channel in  $I_c$  do
12:    if NPC then Skip channel
13:     $x = ptr[ptr\_sh]$ 
14:    for  $s = 0$  to  $O_w$  do
15:      for  $tx = x$  to  $ptr[ptr\_sh + 1]$  do
16:         $\text{convSpMv}(K_h, K_w, O_h, tx, s, IN[tx])$ 
17:       $x = ptr[++ptr\_sh]$ 
```

▷ First value of ptr in each channel
